Mechanism of Viral Glycoprotein Targeting by Membrane-associated-RING-CH Proteins

Cheng Man Lun[1], Abdul A. Waheed[1], Alhlam Majadly[1], Nicole Powell [1], and Eric O. Freed[1*]

[1]Virus-Cell Interaction Section, HIV Dynamics and Replication Program, Center for Cancer Research, National Cancer Institute

*To Whom correspondence should be addressed. Email: efreed@nih.gov

Keywords
E3 ubiquitin ligase, viral glycoproteins, HIV-1 Env, VSV-G, Ebola virus GP, SARS-CoV-2, spike protein, cellular inhibitory factors

Abstract

An emerging class of cellular inhibitory proteins has been identified that targets viral glycoproteins. These include the membrane-associated RING-CH (MARCH) family of E3 ubiquitin ligases that, among other functions, downregulate cell-surface proteins involved in adaptive immunity. The RING-CH domain of MARCH proteins is thought to function by catalyzing the ubiquitination of the cytoplasmic tails (CTs) of target proteins, leading to their degradation. MARCH proteins have recently been reported to target retroviral envelope glycoproteins (Env) and vesicular stomatitis virus G glycoprotein (VSV-G). However, the mechanism of antiviral activity remains poorly defined. Here we show that MARCH8 antagonizes the full-length forms of HIV-1 Env, VSV-G, Ebola virus glycoprotein (EboV-GP), and the spike (S) protein of severe acute respiratory syndrome coronavirus-2 (SARS-CoV-2) thereby impairing the infectivity of virions pseudotyped with these viral glycoproteins. This MARCH8-mediated targeting of viral glycoproteins requires the E3 ubiquitin ligase activity of the RING-CH domain. We observe that MARCH8 protein antagonism of VSV-G is CT-dependent. In contrast, MARCH8-mediated targeting of HIV-1 Env, EboV-GP and SARS-CoV-2 S protein by MARCH8 does not require the CT, suggesting a novel mechanism of MARCH-mediated antagonism of these viral glycoproteins. Confocal microscopy data demonstrate that MARCH8 traps the viral glycoproteins in an intracellular compartment. We observe that the endogenous expression of *MARCH8* in several relevant human cell types is rapidly inducible by type I interferon. These results help to inform the mechanism by which MARCH proteins exert their antiviral activity and provide insights into the role of cellular inhibitory factors in antagonizing the biogenesis, trafficking, and virion incorporation of viral glycoproteins.

Importance

Viral envelope glycoproteins are an important structural component on the surface of enveloped viruses that direct virus binding and entry and also serve as targets for the host adaptive immune response. In this study, we investigate the mechanism of action of the MARCH family of cellular proteins that disrupt the trafficking and virion incorporation of viral glycoproteins across several virus families. This research provides novel insights into how host cell factors antagonize viral

51 replication, perhaps opening new avenues for therapeutic intervention in the replication of a
52 diverse group of highly pathogenic enveloped viruses.
53

54 **INTRODUCTION**
55
56 Viruses rely heavily on host cellular machinery to replicate due to their relatively limited coding
57 capacity. In turn, cells have evolved extensive and elaborate defense mechanisms to impede virus
58 replication. Cells encode numerous proteins, often referred to as inhibitory or restriction factors,
59 that are central components of the innate immune response that serves as the first line of defense
60 against invading pathogens. Well characterized restriction factors include apolipoprotein B
61 mRNA editing catalytic polypeptide-like (APOBEC) family proteins, tripartite motif protein 5 α,
62 (TRIM5α), SAM and HD domain-containing protein 1 (SAMHD1), Myxovirus resistance
63 2 (Mx2), and tetherin/BST-2 (1). These restriction factors are either expressed constitutively
64 and/or are induced by IFN (2-4). Recently, an emerging class of host proteins have been shown to
65 specifically target the synthesis, trafficking and/or function(s) of viral glycoproteins (5). These
66 include the IFN-induced transmembrane (IFITM) proteins, guanylate-binding proteins (GBPs),
67 endoplasmic reticulum class I α-mannosidase (ERManI), galectin 3 binding protein
68 (LGALS3BP/90K), Ser incorporator (SERINC), and the MARCH proteins (5-13).
69 Viral envelope glycoproteins, which are important structural components decorating the
70 surface of enveloped virus particles, recognize receptors on target cells and mediate viral entry by
71 catalyzing membrane fusion events either at the plasma membrane or in low-pH endosomes
72 following endocytic uptake of the viral particle. They are synthesized and cotranslationally
73 glycosylated in the ER and then traffic through the secretory pathway to the site of virus assembly
74 (14). During trafficking through the Golgi apparatus, some viral glycoproteins are cleaved by furin
75 or furin-like proteases as a requisite step in the generation of the fusion-active viral glycoprotein
76 complex. Viral glycoproteins often multimerize (e.g., as trimers) during trafficking (14). Many
77 enveloped viruses assemble at the plasma membrane, whereas some assemble in alternative
78 compartments. For example, SARS-CoV-2 particles are thought to assemble in the ER/Golgi
79 intermediate compartment (ERGIC) and be released by exploiting lysosomal organelles (15, 16).

80 Ubiquitin is a small, 76-amino acid protein that is highly expressed in eukaryotic cells. It
81 can be attached to target proteins, usually on Lys residues, but occasionally on Ser, Thr, or Cys
82 residues, via a multi-enzyme cascade involving an E1 ubiquitin-activating enzyme, an E2
83 ubiquitin-conjugating enzyme, and an E3 ubiquitin ligase (17). Ubiquitin attachment can serve

84 as a signal for target protein degradation in the proteasome or lysosome, or can regulate the
85 endocytic trafficking of the target protein or other aspects of protein function.

86 The MARCH family of RING-finger E3 ubiquitin ligases comprise 11 structurally diverse
87 members. With the exception of the cytosolic MARCH7 and MARCH10 proteins, MARCH
88 family members are transmembrane proteins containing multiple (ranging from 2-14) putative
89 membrane-spanning domains and bearing an N-terminal cytoplasmic RING-CH domain (Fig. 1)
90 (18). MARCH proteins were originally discovered as cellular homologs of the K3 and K5 E3
91 ubiquitin ligases of Kaposi's sarcoma-associated herpes virus (KSHV) (19, 20). These viral
92 MARCH protein homologs confer escape from the host immune response by downregulating the
93 major histocompatibility class I (MHC-I) antigen on the surface of virus-infected cells (21, 22).
94 Other large DNA viruses encode analogous proteins involved in immune evasion (23). Cellular
95 MARCH proteins have been reported to downregulate numerous proteins, including MHC-II (24),
96 transferrin receptor (25), TRAIL receptors (26), CD44 and CD81 (27), IL-1 receptor accessory
97 protein (28), CD98 (29), and tetherin/BST-2 (30). The RING-CH domain of MARCH proteins,
98 and its interaction with E2 enzymes, are responsible for their E3 ligase activity; thus, mutations
99 that either inactivate the catalytic center of the RING domain, or prevent interaction with E2s,
100 abrogate MARCH protein activity (18, 25, 28). MARCH proteins and their viral homologs
101 generally catalyze the transfer of ubiquitin to Lys residues in the CTs of their target proteins,
102 leading to their degradation and/or altered trafficking (18, 19, 25, 31-34). However, the viral
103 MARCH protein homologs K3 and K5 of KSHV have been reported to attach ubiquitin to Ser,
104 Thr, and/or Cys residues (35-37).
105 MARCH8 was first identified in a genome-wide siRNA screen as a potential HIV-1
106 restriction factor acting early in the virus replication cycle by an unknown mechanism (38). More
107 recently, three MARCH proteins – MARCH1, 2 and 8 – were reported to be late-acting restriction
108 factors that target retroviral Env glycoproteins and VSV-G, thereby impairing infectivity of HIV-
109 1 virions bearing these viral glycoproteins (6, 8, 11). The endogenous expression of MARCH
110 proteins differs among cell types, with higher expression of MARCH1, 2 and 8 observed in
111 myeloid cells such as monocyte-derived macrophages (MDM) and monocyte-derived dendritic
112 cells (MDDCs) compared to primary $CD4^+$ T cells (6, 11). MARCH8 expression has been reported
113 to be particularly high in the lung (19). MARCH8 knockdown or knockout in myeloid cells

114 increases HIV-1 infectivity, suggesting that MARCH8 may serve as an antiviral factor in these
115 cell types (11). MARCH1, 2, and 8 are reported to be localized to lysosomes, endosomes and the
116 plasma membrane (18, 19, 25).

117 To understand the mechanism of MARCH-mediated antiviral activity in greater detail,
118 envelope glycoproteins from four families of viruses were selected for study: the retrovirus HIV-
119 1, the rhabdovirus VSV, the filovirus Ebola virus (EboV) and the coronavirus severe acute
120 respiratory syndrome coronavirus-2 (SARS-CoV-2). Three of the glycoproteins encoded by these
121 viruses [HIV-1 Env, EboV-GP, and SARS-CoV-2 spike (S) protein] are cleaved by furin, whereas
122 VSV-G is not (39-41) (Fig.1). HIV-1 Env is synthesized as a precursor, gp160, that is cleaved to
123 gp120 and gp41; the EboV-GP precursor pre-GP is cleaved to GP1 and GP2, and the SARS-CoV-
124 2 S protein precursor is cleaved to S1 and S2 [Fig.1; (39-41)]. The CTs of the viral glycoproteins
125 investigated in this study are highly variable in length, with those of HIV-1 Env, SARS-CoV-2 S
126 protein, VSV-G, and EboV-GP containing 150, 39, 21 and 4 amino acids, respectively (**Fig. 1**).
127 These viral glycoproteins have CTs that vary not only in length but also in the number of Lys
128 residues they contain, with two Lys residues in the CT of HIV-1 Env, four in the SARS-CoV-2 S
129 protein, five in VSV-G, and one in the CT of EboV-GP (Fig. 1). These Lys residues could
130 potentially serve as targets for MARCH-mediated ubiquitination. Our data demonstrate that each
131 of the viral glycoproteins examined is antagonized, to variable extents, by MARCH8. We
132 observed that MARCH-mediated inhibition of VSV-G is CT dependent, whereas inhibition of
133 HIV-1 Env, EboV-GP and SARS-CoV-2 S protein is CT independent. We further demonstrate
134 that knock-down of endogenous *MARCH8* gene expression in HEK293T cells increases the
135 infectivty of HIV-1 particles produced from those cells and that endogenous expression of
136 *MARCH8* is induced by IFN treatment in a human T-cell line, hPBMCs, and primary human
137 airway epithelial cells. Finally, we show that MARCH proteins colocalize with, and retain, the
138 viral glycoproteins in an aberrant intracellular compartment that bears the lysosomal marker
139 LAMP-1. Collectively, our data provide novel insights into the mechanism of action of the
140 MARCH family of cellular E3 ubiquitin ligases and their ability to antagonize diverse viral
141 envelope glycoproteins.
142
143

144 **RESULTS**
145
146
147 **MARCH-mediated inhibition of viral envelope glycoproteins exhibits differential CT**
148 **dependence**. It has been shown that the ectopic expression of MARCH8 in virus-producer cells
149 markedly reduces the infectivity of HIV-1 virions bearing retroviral Env glycoproteins or VSV-G
150 (6, 11). However, the molecular mechanism by which MARCH8 targets viral glycoproteins is not
151 well defined. As mentioned in the Introduction, it has been determined that MARCH proteins
152 downregulate a number of proteins by transferring ubiquitin to their CTs, leading to their
153 lysosomal degradation. To investigate the potential role of MARCH-mediated CT ubiquitination
154 in the downregulation of viral glycoproteins, we deleted the CTs of HIV-1 Env, VSV-G, EboV-
155 GP, and SARS-CoV-2 S protein (**Fig. 1**) and cotransfected the viral glycoprotein expression
156 vectors with the Env(-) pNL4-3 derivative pNL4-3/KFS (42) or a luciferase-encoding NL4-3-
157 derived vector virus. In the case of HIV-1, we used full-length pNL4-3 expressing WT Env or the
158 CT-truncated Env mutant, CTdel-144 (43). Virus-containing supernatants were harvested,
159 normalized for p24 capsid content or reverse transcriptase (RT) activity, and used to infect the
160 TZM-bl indicator cell line (44) or, in the case of the S protein pseudotypes, HEK293T cells stably
161 expressing the human angiotensin converting enzyme 2 (hACE2) receptor. Consistent with
162 previous reports (6, 11), we observed that the infectivity of HIV-1 virions bearing VSV-G was
163 markedly reduced (by ~10-fold) upon expression of WT MARCH8 in the virus-producer cells
164 (**Fig. 2A**). In contrast, the MARCH8-CS (25) and MARCH8-W114A (28, 45, 46) mutants, which
165 abolish RING-CH function or interaction with E2 ubiquitin conjugating enzyme, respectively, did
166 not exert antiviral activity (**Fig. 2A**). We observed that the infectivity conferred by VSV-G Tailless
167 was ~40% that of WT VSV-G, and overexpression of MARCH8 in virus-producer cells had no
168 significant effect on the infectivity of this VSV-G variant (**Fig. 2A**). Next, we investigated the
169 ability of MARCH8 to inhibit a VSV-G mutant in which the Lys residues in the CT, which are
170 potential sites of MARCH8-mediated ubiquitination, were substituted. A VSV-G mutant in which
171 the five Lys residues in the CT were mutated to Ala displayed severely compromised infectivity
172 (data not shown). We therefore introduced the more conservative Lys-to-Arg substitution (K-to-
173 R) at these five Lys residues (Fig. 1) and observed that this mutant is fully infectious relative to
174 the WT. As observed with the VSV-G Tailless mutant, overexpression of MARCH8 in virus-
175 producer cells had no significant effect on the infectivity of the VSV-G K-to-R mutant. As

176 expected, the MARCH8 mutants likewise did not diminish the infectivity of either the Tailless or
177 K-to-R VSV-G mutants. These results indicate that the ability of MARCH8 to antagonize VSV-G
178 in this experimental system is dependent upon the Lys residues in the VSV-G CT, likely because
179 they are targets of MARCH8-mediated ubiquitination.

180 As reported previously (6, 11), we observed that the infectivity of virus particles bearing
181 HIV-1 Env is severely reduced (by ~10-fold) upon overexpression of WT MARCH8 in the virus-
182 producer cell. This inhibitory activity was to a large extent eliminated by the MARCH8-CS and
183 MARCH8-W114A mutations (**Fig. 2B**). To investigate whether the inhibition of HIV-1 Env is CT
184 dependent we tested the CTdel144 Env mutant (43), which lacks nearly the entire gp41 CT (**Fig.**
185 **1**). Under these assay conditions, the infectivity of CTdel144 HIV-1 was ~40% that of WT HIV-
186 1. Interestingly, in contrast to the lack of MARCH8-mediated inhibition observed with Tailless
187 VSV-G, the infectivity of CT-deleted HIV-1 was reduced to a similar extent as the WT by
188 expression of MARCH8 in the virus-producer cells. The MARCH8 mutants did not significantly
189 inhibit the infectivity of the CTdel144 HIV-1 Env mutant. These results demonstrate that
190 MARCH8-mediated antagonism of HIV-1 Env requires the E3 ubiquitin ligase activity of the
191 RING domain but does not require the gp41 CT.

192 As indicated above, the dependency on the CT for MARCH8-mediated inhibition differs
193 between VSV-G and HIV-1 Env. We next examined the effect of MARCH8 on the infectivity of
194 the EboV-GP, which contains a CT of only four amino acids (**Fig. 1**). For these experiments, we
195 used a version of the EboV-GP lacking the mucin-like domain (47) as we obtained higher
196 infectivity with this variant (data not shown). We will refer to this delta mucin-like domain variant
197 (ΔMLD) as WT because it contains an intact CT. The infectivity of HIV-1 virions bearing either
198 the WT or CT-deleted EboV-GP was reduced by ~30-40 % when the virus was produced in the
199 presence of MARCH8. We also mutated the single Lys residue in the CT of EboV-GP and
200 observed that the infectivity of this K-to-A mutant was inhibited by ~50% in the presence of
201 MARCH8. The infectivity of EboV-GP mutants was similar to that of the WT in the absence of
202 MARCH8 overexpression (**Fig. 2C**). No statistically significant reduction in infectivity was
203 observed for WT EboV-GP upon expression of the MARCH8-CS mutant, yet a minor reduction
204 in infectivity was observed for EboV-GP Tailless and K-To-A mutants in the presence of the
205 MARCH8-W114A mutant (**Fig. 2C**). These results demonstrate that MARCH8-mediated

206 antagonism of EboV-GP is dependent on the E3 ubiquitin ligase activity of the RING domain but
207 does not require the short EboV-GP CT.

208 We next tested the effect of MARCH8 overexpression on the infectivity of particles bearing
209 the SARS-CoV-2 S protein, which has a 39 amino acid CT with five Lys residues. We also tested
210 a CT-truncated SARS-CoV-2 S protein, which bears a 19 amino acid truncation and contains one
211 Lys residue (**Fig. 1**). The infectivity of HIV-1 virions bearing WT or CT-truncated SARS-CoV-2
212 S protein was reduced by ~60% in the presence of MARCH8. We also mutated the Lys residues
213 in the CT of both WT and CT-truncated SARS-CoV-2 S proteins and observed ~50% reductions
214 in particle infectivity upon overexpression of MARCH8 in the virus-producer cell. The infectivity
215 of particles bearing truncated or Lys-mutant SARS-CoV-2 S proteins was modestly higher than
216 those bearing the WT S protein, likely due to disruption of the endoplasmic reticulum (ER)-
217 retention signal in the CT (48-50) (**Fig. 2D**). Expression of the inactive MARCH8-CS mutant
218 did not reduce the infectivity of particles bearing the WT SARS-CoV-2 S protein or the full-length
219 K-to-R mutant, but it did cause some reduction in the infectivity of virions bearing the CT-
220 truncated forms of SARS-CoV-2 S protein (**Fig. 2D**).

221 We note that the effect of MARCH8 expression on the infectivity of particles bearing
222 EboV-GP or SARS-CoV-2 S protein is modest relative to its effect on the infectivity of particles
223 bearing VSV-G or HIV-1 Env. To investigate whether different levels of EboV-GP or SARS-
224 CoV-2 S protein expression would affect the MARCH8-mediated inhibition of pseudotype
225 infectivity, we performed transfections with a range of viral glycoprotein expression vector inputs.
226 In the case of EboV-GP, we observed a 40-50% reduction in pseudotyped particle infectivity
227 across the range of GP expression vector inputs (from 100-600 ng). In contrast, with SARS-CoV-
228 2, we observed a 4-fold reduction in infectivity with 100 ng input, but a more-modest 2-fold
229 reduction with a 400 ng input (data not shown).

230 Altogether, the data presented in Fig. 2 demonstrate that MARCH8 overexpression in the
231 virus-producer cell inhibits the infectivity of virus particles bearing each of the four viral
232 glycoproteins tested. The inhibitory activity of MARCH8 is largely abrogated by mutations
233 reported to block E3 ubiquitin ligase activity (CS and W114A), although some residual inhibitory
234 activity was observed with these mutants in some assays. Importantly, in the case of VSV-G,
235 MARCH8-mediated inhibition is dependent on the Lys residues in the CT, whereas inhibition of
236 HIV-1 Env, EboV-GP, and SARS-CoV-2 S protein does not require the CT.

237

238 **MARCH8 expression in virus-producer cells leads to viral envelope glycoprotein**
239 **degradation and reduced processing and virion incorporation.** To investigate the mechanism
240 by which MARCH8 expression reduces the infectivity of virus particles bearing VSV-G we
241 transfected 293T cells with the Env(-) pNL4-3 molecular clone pNL4-3/KFS and the WT or
242 mutant VSV-G expression vectors, with or without MARCH8 expression vectors. VSV-G levels
243 in cell and virion fractions were quantified by western blot (WB). Cotransfection with an
244 expression vector for FLAG-tagged small glutamine-rich tetratricopeptide repeat-containing
245 protein (SGTA) provided a loading control. As shown in **Fig. 3A**, overexpression of WT
246 MARCH8 markedly reduced (by ~3-fold) the expression of VSV-G in both cell and virion
247 fractions. Consistent with the lack of inhibition observed with the MARCH8-CS and MARCH8-
248 W114A mutants in the infectivity assays (**Fig. 2**), significant reductions in VSV-G levels were not
249 observed with these MARCH8 mutants (**Figs. 3A and 3B**) despite comparable WT and mutant
250 MARCH8 expression levels (**Fig. 3A**). Also consistent with the infectivity data, overexpression of
251 WT or mutant MARCH8 did not significantly affect levels of Tailless or K-to-R VSV-G mutants
252 in either cell or virus fractions. We also observed that overexpression of MARCH8 had no
253 significant effect on the expression of viral Gag proteins in cells or on virus release, which, together
254 with the observed lack of effect on SGTA expression levels, indicated that the reduction of VSV-
255 G levels in the presence of MARCH8 is not due to cytotoxicity or globally reduced protein
256 expression. Finally, we observed a more rapid mobility of VSV-G in the presence of WT but not
257 mutant MARCH8, presumably due to reduced VSV-G glycosylation induced by MARCH8
258 expression (Fig. 3A). This effect on VSV-G mobility was not observed with the Tailless or K-to-
259 R mutants, consistent with these mutants being resistant to MARCH8-mediated inhibition.

260 To measure the half-life of VSV-G in the presence or absence of MARCH8, we performed
261 pulse-chase analysis. 293T cells expressing WT VSV-G alone, or coexpressing VSV-G with
262 MARCH8, were pulse-labeled with [^{35}S]Met/Cys for 20 min and chased for 0, 2, or 4 h in
263 unlabeled medium. We observed that MARCH8 overexpression reduced the levels of VSV-G, on
264 average, to 52% and 34% at 2 and 4 h, respectively, compared to 85% and 78% in the absence of
265 MARCH8 at those time points (**Fig. 3C**). These results indicate that MARCH8 overexpression
266 promotes the degradation of VSV-G, leading to reduced expression in cells and incorporation into
267 virions.

268 Similar experiments to those described above were performed with HIV-1 Env. MARCH8
269 expression significantly reduced the levels of both gp120 and gp41 in virions. The incorporation
270 of WT gp120 was not impaired by expression of the MARCH8 mutants, while the MARCH8-
271 W114A mutant modestly reduced (by ~40%) the levels of virion-associated gp120 for CTdel144
272 Env. The levels of virion-associated gp41 were markedly reduced for both WT and CTdel144 Env
273 in the presence of MARCH8, and the MARCH8 mutants did not exert a statistically significant
274 effect on virion gp41 levels (**Fig. 4A and C**). The reduced levels of virion-associated gp120 and
275 gp41 imposed by MARCH8 expression are consistent with the infectivity data presented above
276 (**Fig. 2B**). The expression of exogenous FLAG-tagged SGTA and HIV-1 Gag proteins in cells
277 was similar across the different transfected samples, indicating that expression of WT and mutant
278 MARCH8 is not cytotoxic under these conditions and no effect on virus particle production was
279 observed (**Fig. 4A**). These results demonstrate that MARCH8 expression in the virus-producer
280 cell reduces the levels of virion-associated gp120 and gp41 for both WT and gp41 CT-deleted
281 HIV-1 Env.
282 The EboV-GP bears a CT that contains only four residues, considerably shorter than the
283 CTs of either VSV-G or HIV-1 Env, yet it resembles HIV-1 Env in terms of the CT-independence
284 of its inhibition by MARCH8 in infectivity assays (**Fig. 2**). To investigate the effect of MARCH8
285 expression on the processing and incorporation of EboV-GP, we analyzed the levels of cell- and
286 virion-associated EboV-GP in the presence and absence of MARCH8. The levels of cell- and
287 virion-associated EboV-GP were significantly reduced in the presence of WT MARCH8, but not
288 in the presence of the MARCH8-CS or MARCH8-W114A mutants (**Fig. 5A and C**). The
289 incorporation of the Tailless and K-to-A EboV-GP mutants was also reduced in the presence of
290 MARCH8 (**Fig. 5A and B**). We observed a significant reduction in the processing of EboV-GP0
291 in the presence of WT but not mutant MARCH8, as determined by the ratio of cell-associated
292 GP0/GP1 (**Fig. 5A and D**). As observed with VSV-G and HIV-1 Env, overexpression of WT or
293 mutant MARCH8 had no significant effect on cell-associated Gag expression or particle
294 production (**Fig. 5A**). These observations demonstrate that the MARCH8-mediated infectivity
295 defect observed with EboV-GP is due to impaired GP0 processing and correspondingly reduced
296 virion incorporation of GP1 and GP2, and this defect is independent of the EboV-GP CT.
297 As mentioned in the Introduction, MARCH8 expression has been reported to be high in
298 the lung (51), making its effect on the respiratory virus SARS-CoV-2 of particular interest.

299 Because the experiments described above demonstrated that neither inactive MARCH8 mutant
300 (MARCH8-CS or MARCH8-W114A) was capable of consistent antiviral activity, in these and
301 subsequent experiments we used only one mutant, MARCH8-CS, as our negative control. As
302 observed with HIV-1 Env and EboV-GP, the SARS-CoV-2 S protein shows a CT-independent
303 MARCH8-mediated restriction in infectivity assays (**Fig. 2**). To examine the effect of MARCH8
304 on SARS-CoV-2 S protein expression, we analyzed the levels of cell- and virion-associated S
305 protein in the presence and absence of WT or catalytically inactive MARCH8. We observed that
306 MARCH8 expression significantly reduced (by ~3-4 fold) the levels of S2 in cells and reduced S2
307 levels by ~10-fold in virions. Averaged over multiple assays, the MARCH8-CS mutant did not
308 significantly reduce S protein levels (**Fig. 6A and C**). Consistent with the infectivity data
309 presented above, the levels of the S protein mutants (K-to-R, CT-truncated, and CT-truncated K-
310 to-R) were also reduced in the presence of MARCH8. We also observed a 60-70% reduction in
311 the levels of WT and mutant S2 in the cell fraction in the presence of MARCH8, and noted the
312 presence of a smaller S2-related protein product (**Fig. 6A, red arrow**), which we speculate to be
313 a less-glycosylated form of S2. The reductions in S2, and the presence of the smaller S2 species,
314 were not observed upon expression of the MARCH8-CS mutant (**Fig. 6A and B**). Levels of the S
315 precursor protein were not reduced by expression of MARCH8 in the virus-producer cell,
316 suggesting an effect primarily on S protein processing. These data demonstrate that expression of
317 WT MARCH8 but not the MARCH8-CS mutant disrupts S protein processing, glycosylation, and
318 incorporation into virus particles and indicate that the MARCH8-imposed antagonism of SARS-
319 CoV-2 S protein is CT independent.
320 Because the effect of MARCH8 expression on both particle infectivity and glycoprotein
321 levels in virions varied across the four viral glycoproteins studied here, we calculated the
322 incorporation efficiency of each glycoprotein under the conditions used in the experiments
323 described above (**Fig. S2**). We observed that the Ebo-GP incorporation efficiency was quite high,
324 with nearly 40% of expressed GP present in VLPs. In contrast, the incorporation of SARS-CoV-
325 2 S protein was quite low, perhaps because HIV-1 particles assemble on the plasma membrane,
326 which, as noted in the Introduction, is not the normal site of SARS-CoV-2 assembly. Incorporation
327 efficiencies of HIV-1 gp41 and VSV-G were ~18% and ~8%, respectively, under these
328 experimental conditions (**Fig. S2**).
329

330 **Knockdown of endogenous MARCH8 expression in HEK293T increases HIV-1 infectivity.**

331 Although levels of basal MARCH8 expression are known to be relatively low in
332 established cell lines (51). We examined whether knock-down of *MARCH8* gene expression in
333 HEK293T cells would affect the infectivity of HIV-1 particles produced from the *MARCH8*-
334 depleted cells. HEK293T cells were treated with siRNA targeting MARCH8 or with a non-
335 targeting control. *MARCH8* expression was measured by RT-qPCR. At the highest siRNA input,
336 *MARCH8* gene expression was reduced by approximately 5-fold (**Fig. 7A**). Under these
337 conditions, we observed a modest but statistically significant increase in the infectivity of HIV-1
338 particles produced from the *MARCH8*-depleted cells (**Fig. 7B**). The infectivity of virus produced
339 from cells treated with the non-targeting siRNA control was not affected. These results
340 demonstrate that even low levels of endogenous MARCH8 expression can impair HIV-1
341 infectivity.

342

343 ***MARCH8* expression is highly and rapidly inducible in certain cell types by IFN stimulation.**
344 Previous findings demonstrated that MARCH8 is highly expressed in MDMs in the
345 absence of IFN stimulation and that expression levels are not appreciably increased in either
346 MDMs or human $CD4^+$ T cells by overnight stimulation with IFN-α (11). Because IFN is known
347 to induce highly variable levels of gene expression in a time-, dose-, and cell type-dependent
348 manner (52, 53), and many genes with antiviral functions are IFN inducible (54), we performed
349 RT-qPCR time-course experiments with three different IFNs [IFN type-I (α and *β*) and II (γ)]
350 using total RNA extracted from different cell types and cell lines. We tested the SupT1 human T-
351 cell line, primary hPBMCs from four different donors, the A549 transformed alveolar epithelial
352 cell line, primary human airway epithelial cells, and HEK293T cells. In the SupT1 T-cell line,
353 *MARCH8* gene expression was rapidly induced at 0.5 hr post-stimulation with IFN-α up to 70-
354 fold over baseline levels, which subsided to ~10-fold over unstimulated levels by 4 hrs after
355 induction (**Fig. 7A**) and then returned to baseline. Treatment with IFN-β induced a ~30-fold
356 increase in *MARCH8* gene expression over baseline that peaked around 1-2 hrs post-IFN
357 stimulation (**Fig. 7A**). To examine *MARCH8* gene expression in primary hPBMCs, cells from
358 four donors were IFN stimulated and *MARCH8* RNA levels measured. In three of the four donors,
359 we observed that *MARCH8* expression increased 5-8-fold over unstimulated levels at 0.5 hr post-

360 stimulation with IFN-α and then returned to baseline by 2 hr post-stimulation (**Fig. 7B**). In one
361 donor, no IFN-inducible *MARCH8* gene expression was observed (data not shown). To investigate
362 *MARCH8* gene expression in cells that are permissive for SARS-CoV-2 infection, we tested
363 primary human airway epithelial cells and observed a ~3-fold increase in expression at 1-4 h post
364 IFN-α stimulation (**Fig. 7C**). In HEK293T cells, we measured a rapid, ~7-fold increase in
365 MARCH8 gene expression after stimulation with IFN-α. Finally, we observed no IFN stimulation
366 of *MARCH8* gene expression in A549 cells (data not shown). Collectively, these data indicate that
367 *MARCH8* gene expression is induced to varying levels in cell lines and primary cells types that are
368 natural targets for HIV-1 and SARS-CoV-2 infection.
369 It is important to verify that the levels of exogenous *MARCH8* gene expression achieved
370 in these assays were not excessive relative to endogenous levels present in relevant cell types.
371 Therefore, we investigated the *MARCH8* RNA expression levels in transiently transfected
372 HEK293T cells upon increasing MARCH8 concentrations at 48 hr post-transfection. The results
373 indicated that *MARCH8* expression at 0.05 and 0.1 μg DNA input, the conditions used for the
374 analyses presented in Figs. 2-6, was ~4-5 fold above the levels in untransfected cells (**Fig. 8E**).
375 Transfection efficiencies were ~50% under these conditions (data not shown), indicating that
376 transfected cells expressed *MARCH8* RNA at levels that were ~8-10 fold over those of
377 untransfected cells. These results show that exogenous levels of *MARCH8* gene expression in our
378 transfected 293T cells were lower than those observed following IFN stimulation of the SupT1 T-
379 cell line and comparable to those measured in some IFN-stimulated hPBMC donors and HEK293T
380 cells at early time points after IFN stimulation (**Fig. 8 A-D**). The levels of basal expression of
381 *MARCH8* relative to the house-keeping gene *GAPDH* in all of these cell types were comparable
382 (**Table S1**). Collectively, our data demonstrate that *MARCH8* gene expression can be induced
383 rapidly by IFN stimulation in different cell types: a human T-cell line, hPBMCs, human airway
384 epithelial cells and the HEK293T cell line. The levels of exogenous expression in our transfected
385 HEK293T cells were lower than, or comparable to, those achieved upon IFN stimulation at early
386 time points in the T-cell line, primary hPBMCs, and HEK293T cells.
387
388 **MARCH8 retains VSV-G, HIV-1 Env, EboV-GP and SARS-CoV-2 S protein in an**
389 **intracellular compartment.** The western blotting data presented above demonstrate that
390 MARCH8 overexpression disrupts the processing and incorporation of viral envelope

391 glycoproteins, suggesting that MARCH8 might alter the trafficking of these viral glycoproteins.
392 To examine the effect of MARCH8 overexpression on the localization of different viral
393 glycoproteins, we performed confocal microscopy using HEK293T cells transfected with
394 MARCH8 or the inactive MARCH8-CS mutant. Our confocal data showed that MARCH8
395 localizes to the Golgi, a LAMP-1$^+$ compartment, and the plasma membrane (**Fig. S1**) as previously
396 reported (51). All of the viral glycoproteins and mutants used in this study colocalized with
397 MARCH8 and MARCH8-CS with strong Pearson's correlation coefficients (r) of ~0.7- 0.9 (Table
398 1) indicating that MARCH proteins and viral glycoproteins traffic through the same pathway. We
399 quantified the intracellular colocalization between the dsRed-Golgi marker and the different viral
400 glycoproteins in the presence of WT MARCH8 and the inactive MARCH8-CS and observed
401 strong colocalization (r=~0.7-0.9) (**Table 1, Fig. 9 to 12**).

402 In the absence of MARCH8 overexpression, we observed WT VSV-G localization
403 primarily in the Golgi and at the plasma membrane (**Fig. 9A**). MARCH8 but not MARCH8-CS
404 expression resulted in a marked shift in the localization of WT VSV-G from the plasma membrane
405 to an intracellular vesicular compartment (**Fig. 9A**). The predominantly plasma membrane
406 localization of the VSV-G Tailless (**Fig. 9B**) and VSV-G K-to-R (**Fig. 9C**) mutants was not shifted
407 by MARCH8 expression, consistent with the lack of MARCH8 targeting of these VSV-G mutants
408 in infectivity and western blotting analyses. We observed a strong colocalization (r ~ 0.89)
409 between WT VSV-G and the lysosomal marker LAMP-1 in the presence of WT MARCH8
410 expression (**Fig. 9D; Table 1**), whereas the Tailless and K-to-R VSV-G mutants showed low levels
411 of colocalization with LAMP-1 (r ~ 0.2). In the presence of the inactive MARCH8-CS mutant,
412 neither WT nor mutant VSV-G showed a high level of colocalization with LAMP-1 (r ~ 0.2) (**Fig.
413 9E; Table 1**). These data demonstrate that MARCH8 interferes with VSV-G trafficking and
414 targets it to a LAMP-1-positive compartment in a manner that requires the Lys residues in the
415 VSV-G CT.

416 We performed similar analyses with HIV-1 Env. As expected, WT and CTdel144 HIV-1
417 Env were observed in the Golgi and at the plasma membrane in the absence of MARCH8
418 expression (**Fig. 10A and B**). Similar to VSV-G, localization of WT HIV-1 Env was shifted in
419 cells expressing MARCH8, and a high level of colocalization (r ~0.8) with LAMP-1 was observed
420 (**Fig. 10C; Table 1**). In contrast to VSV-G, for which MARCH8-induced localization required
421 the CT, the Tailless form of HIV-1 Env, CTdel144, was strongly localized to a LAMP-1$^+$

422 compartment in MARCH8-expressing cells (**Fig. 10C; Table 1**). The inactive MARCH8-CS did
423 not result in the retention of either WT or CTdel144 HIV-1 Env in a LAMP-1$^+$ compartment (**Fig.**
424 **10D**). These findings are consistent with the infectivity and western blotting data presented above,
425 and indicate that the reductions in HIV-1 Env processing and incorporation in the presence of
426 MARCH8 are associated with the retention of Env in an internal, LAMP-1$^+$ compartment.
427 The confocal microscopy data obtained with EboV-GP and SARS-CoV-2 S protein
428 paralleled our observations with HIV-1 Env but diverged from the results obtained with VSV-G.
429 Expression of MARCH8 but not MARCH8-CS reduced the expression of these viral glycoproteins
430 on the cell-surface and induced their retention in an internal, LAMP-1$^+$ compartment. The
431 localization of truncated and K-to-R EboV-GP and S protein mutants was also shifted by
432 MARCH8 expression (**Figs. 11 and 12; Table 1**).
433 Taken together, the confocal microscopy data demonstrate that MARCH8 expression
434 redirects the localization of viral glycoproteins by two distinct mechanisms. In the case of VSV-
435 G, the CT is required for the MARCH8-induced relocalization to a LAMP-1$^+$ compartment and
436 mutation of the Lys residues in the CT abrogates the ability of MARCH8 expression to disrupt the
437 localization of the viral glycoprotein. In contrast, for HIV-1 Env, EboV-GP and SARS-CoV-2 S
438 protein, neither the CT nor the Lys residues in the CT are required for MARCH8-induced
439 relocalization. The microscopy data are thus consistent with the infectivity and western blotting
440 data (**Fig. 2-6**) showing that the ability of MARCH8 to antagonize VSV-G is dependent on the CT
441 but the antagonism of the other viral glycoproteins tested is CT independent.
442
443 **DISCUSSION**
444
445 In this study, we examined the ability of MARCH8 to antagonize a wide range of viral
446 envelope glycoproteins – specifically, HIV-1 Env, VSV-G, EboV-GP and SARS-CoV-2 S protein.
447 Expression of MARCH8 in the virus-producer cell reduced levels of viral glycoprotein processing
448 for those glycoproteins that undergo furin-mediated cleavage, reduced glycoprotein stability, and
449 interfered with glycoprotein incorporation into HIV-1 particles. In the case of VSV-G, MARCH8-
450 mediated antagonism required the CT of the viral glycoprotein, and Lys residues in the CT were
451 essential for MARCH8 restriction. In contrast, in the case of HIV-1 Env, EboV-GP, and SARS-
452 CoV-2 S protein, the CT of the viral glycoprotein was not required for the antiviral effect. In all
453 cases, however, the ubiquitin ligase activity of MARCH8 was required for restriction, as RING

454 domain mutations to a large extent abrogated the inhibition. While this manuscript was in
455 preparation, another group reported that, as we observed here, MARCH8-mediated restriction of
456 VSV-G was CT-dependent but antagonism of HIV-1 Env was CT-independent, and they
457 demonstrated MARCH8-mediated ubiquitination of VSV-G (55). These results support a model
458 whereby the RING domain E3 ubiquitin ligase activity of MARCH8 either directly targets the CT
459 of the viral glycoprotein – as has been shown for MARCH protein-mediated downregulation of a
460 variety of cellular proteins (18) – or exerts its effect indirectly. In either case, the consequence of
461 MARCH8 activity is the apparent redirection of the viral glycoproteins to a LAMP-1^{+}
462 compartment. This is consistent with MARCH8 inducing lysosomal degradation of viral
463 glycoproteins.

464 While MARCH8 expression antagonized each of the glycoproteins tested here, the
465 magnitude of the effect varied across the different glycoproteins, in terms of both particle
466 infectivity and glycoprotein incorporation into virions. Specifically, the inhibition of VSV-G and
467 HIV-1 Env was quite severe, whereas more modest effects were observed with EboV-GP and
468 SARS-CoV-2 S. The degree of inhibition did not correlate with the viral glycoprotein
469 incorporation efficiency; for example, EboV-GP was very efficiently incorporated into HIV-1
470 particles, whereas SARS-CoV-2 S protein was inefficiently incorporated. Further study will be
471 required to determine the basis for the variable activity of MARCH8 against the four glycoproteins
472 examined in this study.

473 It remains unclear at what stage during their trafficking pathway viral glycoproteins are
474 targeted by MARCH8. MARCH8 could act early during trafficking of the viral glycoprotein
475 through the Golgi *en route* to the site of virus assembly, at the plasma membrane, or, in the case
476 of glycoproteins like HIV-1 Env that undergo a recycling step, could act late following endocytic
477 uptake from the plasma membrane. MARCH proteins have been reported to target a large
478 repertoire of cellular proteins, including innate/adaptive immune receptors and intracellular
479 adhesion molecules (18). Previous studies have shown that the overexpression of MARCH
480 proteins can cause redistribution of syntaxin 4 and syntaxin 6 as well as some syntaxin-6-
481 interacting soluble *N*-ethylmaleimide-sensitive factor attachment protein receptors (SNAREs),
482 which are known to be involved in cellular endosomal trafficking (56, 57). MARCH protein
483 overexpression has also been reported to alter the trafficking of clathrin-independent endocytosis
484 (CIE) cargo proteins, rerouting them to endosomes and lysosomes for degradation (29). Thus, the

485 indirect mechanism of MARCH8-mediated targeting of viral glycoproteins that we hypothesize
486 would involve the ubiquitination and downregulation of cellular factor(s) involved in viral
487 glycoprotein trafficking. The resulting accumulation of the viral glycoprotein in a LAMP-1$^+$
488 intracellular compartment (Figs. 9-12), would reduce virion incorporation of the viral glycoprotein
489 and impair particle infectivity. Taken together, our data suggest that MARCH8 exerts its antiviral
490 activity via two different mechanisms, one (e.g., as observed for VSV-G) in which the CT of the
491 viral glycoprotein is directly ubiquitinated, the other (e.g., as observed for HIV-1 Env, EboV-GP,
492 and SARS-CoV-2 S) in which host trafficking factor(s) are targeted, resulting in an indirect
493 restriction of the viral glycoprotein.

494 The viral homologs of the cellular MARCH proteins have been reported to ubiquitinate
495 residues other than Lys in the CTs of their target proteins; for example, the K3 protein of KSHV
496 has been reported to attach ubiquitin to Cys residues and the mK3 protein of gamma herpesviruses
497 can ubiquitinate Ser and Thr in addition to Lys (35-37, 58). It is not clear whether MARCH
498 proteins are able to ubiquitinate non-Lys residues, but we cannot exclude this possibility.
499 Inspection of the viral glycoproteins under study indicates that the truncated HIV-1 Env mutant
500 CTdel144 and EboV-GP Tailless have no Ser, Thr or Cys residues facing the cytosol, indicating
501 that their CTs cannot be ubiquitinated. In contrast, SARS-CoV-2 S-Trun has 4 Ser, 1 Thr and 10
502 Cys residues. Ongoing work is investigating whether the CT of SARS-CoV-2 S protein undergoes
503 MARCH8-mediated ubiquitination. It is interesting to note that the basic residues in the CT of
504 HIV-1 gp41 are highly skewed towards Arg instead of Lys residues; for example, the CT of the
505 NL4-3 strain of HIV-1 used in this study contains 21 Arg residues but only two Lys residues
506 (https://www.hiv.lanl.gov/content/sequence/HIV/mainpage.html). This observation invites the
507 speculation that HIV-1 may have evolved to limit the number of Lys residues available for gp41
508 CT ubiquitination.

509 Our results show a broad antiviral activity of MARCH8 against the glycoproteins from
510 three human viral pathogens – HIV-1, EboV, and SARS-CoV-2 – and a primarily animal pathogen,
511 VSV. MARCH8 targeting of HIV-1 Env, VSV-G, and, very recently, EboV-GP, has been reported
512 (6, 8, 11, 55, 59). HIV-1 replicates predominantly in CD4$^+$ T cells and also infects MDM (60).
513 EboV targets mainly alveolar macrophages and endothelial cells (61); SARS-CoV-2, like other
514 coronaviruses, targets airway epithelial cells (62); and VSV typically replicates in cells of the oral
515 mucosa, although VSV-G confers very broad tissue tropism (63). In this study, we relied

516 extensively on expressing MARCH8 exogenously to evaluate its effect on viral envelope
517 glycoprotein stability, trafficking, and incorporation. This raises the question of whether the levels
518 of MARCH8 expression achieved in these experiments are physiologically relevant. A previous
519 study demonstrated that depletion of MARCH8 in primary human MDM significantly increased
520 the infectivity of HIV-1 particles released from these cells, suggesting that at least in this cell type
521 endogenous levels of MARCH8 expression are sufficient to restrict HIV-1 infectivity (11).
522 MARCH8 expression is high in the lung (19), suggesting its potential relevance to infection by
523 respiratory viruses like SARS-CoV-2. Due to the poor quality of available MARCH8 antibodies,
524 we could not evaluate endogenous MARCH8 protein expression. Instead, qRT-PCR was used to
525 measure the endogenous *MARCH8* gene expression in relevant cell types in the presence and
526 absence of IFN. In the absence of IFN stimulation, basal levels of *MARCH8* RNA, measured as a
527 ratio to *GAPDH*, were similar across the cell types analyzed. The RNA levels measured following
528 IFN induction were comparable to those in transiently transfected HEK293T cells. Although RNA
529 levels may not be directly correlated with protein expression, the results suggest that the MARCH8
530 expression in the cell types tested may be sufficient to exert an antiviral activity. Indeed, even in
531 the absence of IFN stimulation, we observed that depletion of MARCH8 in HEK293T cells caused
532 a modest but statistically significant increase in the infectivity of particle produced from those
533 cells. In addition, our data indicate that *MARCH8* is an IFN-stimulated gene (ISG). The type I
534 IFN (IFN-I) response is crucial in the host antiviral defense against viral infections (64, 65). For
535 example, a recent publication highlighted the importance of the IFN-I response in immune
536 protection against SARS-COV-2 by establishing a link between life-threatening COVID-19
537 symptoms and loss-of-function mutations in IFN-I-related genes (66).
538 Viruses, including those whose envelope glycoproteins were studied here, have evolved a
539 complex array of countermeasures to disable the function of cellular ISGs (67) . Further work will
540 be required to elucidate mechanisms by which viruses counteract the antiviral activity of the
541 MARCH family of E3 ubiquitin ligases.
542

543 **Materials and Methods**
544
545 **Cell culture**. HEK293T cells [obtained from the American Type Culture Collection (ATCC) and
546 TZM-bl cells (obtained from J. C. Kappes, X. Wu, and Tranzyme, Inc. through the NIH AIDS
547 Reagent Program (ARP), Germantown, MD)] were maintained in DMEM containing 5% or 10%
548 (vol/vol) fetal bovine serum (FBS; HyClone), 2mM glutamine, 1% penicillin-streptomycin
549 (penicillin 50 U/ml and streptomycin 50 µg/ml, final concentration; Lonza) at 37 °C with 5% CO_2.
550 The SupT1 T-cell line was cultured in RPMI with 10% FBS and 1% penicillin-streptomycin. The
551 A549 human lung epithelial cell line (obtained from the ATCC) was cultured in DMEM with 10%
552 FBS and 1% penicillin-streptomycin. Primary small airway epithelial cells (obtained from ATCC)
553 were cultured in airway epithelial cell basal medium (ATCC) supplemented with bronchial
554 epithelial cell growth kit (ATCC). Primary hPBMC were obtained from healthy volunteers from
555 the NCI-Frederick Research Donor Program. The hPBMCs were extracted from whole blood
556 using Histopaque procedure (Sigma). Cells were then stimulated with PHA-P and IL-2 for three
557 days.
558
559 **Plasmids and transfection.** The following plasmids were used in this study: the full-length HIV-
560 1 clade B molecular clone pNL4-3 and derivatives pNL4-3EnvCTdel144 (68), pNL4-3KFS (*env*-
561 minus) (69), pNL4-3.Luc.R-E- (NIH ARP, #3418); and the pHCMV-G (VSV-G expression
562 vector) (70, 71). The EboV-GP ΔMLD was a gift from Judith White (University of Virginia) (47)
563 and SARS-CoV-2 S protein (FL and Truncated) expression vectors were gifts from Thomas
564 Gallagher (Loyola University). Viral glycoprotein mutant plasmids VSV-G Tailless, VSV-G K-
565 to-A and VSV-G K-to-R; EboV-GP-K-to-A and EboV-GP-Tailless; SARS-CoV-2 S-FL-K-to-R
566 and SARS-CoV-2 S-Truncated-K-to-R) were generated using the Q5® site-directed mutagenesis
567 kit (New England BioLabs Inc., #E0552S) or the QuickChangeSite-Directed Mutagenesis kit
568 (Stratagene) according to the manufacturer's instructions with primers listed in Table S1. In
569 microscopy experiments, pDsRed-monomer-Golgi-Beta-1,4-galactosyltransferase (Clontech,
570 #632480) and LAMP-RFP (Addgene, #1817) (72) were used. Plasmids were purified using
571 MaxiPrep Kits (Qiagen, #12263) and mutations were verified by sequencing (Psomagen,
572 Rockville, MD). The HEK293T cells were transfected with the indicated plasmids using PEI or
573 Lipofectamine 2000 (Invitrogen) according to manufacturer's instructions. Virus-containing
574 supernatants were filtered through 0.45-µm membrane 24 or 48 hours post-transfection and virus

575 was quantified by measuring RT activity. Virus-containing supernatant was harvested 24 or 48
576 hours post-transfection and virus particles were collected by ultracentrifugation. Virus and cell
577 pellets were solubilized in lysis buffer (10mM iodoacetamide (Sigma-Aldrich), Complete^{TM}
578 protease inhibitor tablets (Roche), 300 mM sodium chloride, 50mM Tris-HCl (pH 7.5) and 0.5%
579 Triton X-100 (Sigma-Aldrich)) and used for further analysis.
580
581 **Western blotting.** Cell and virus lysates in lysis buffer with 6x SDS-PAGE sample loading buffer
582 (600 mM Tris-HCL pH6.8, 30% glycerol, 12% SDS, 20mM DTT, 0.03% bromophenol blue) were
583 heated at 95°C for 5 min. Samples were analyzed on 10% 1.5mm Tris-glycine gels using a BioRad
584 Trans-Blot Turbo Transfer system according to manufacturer's instructions. Proteins were
585 detected with primary antibodies (see Table S2) and secondary antibodies. Protein bands were
586 visualized using chemiluminescence with either a Gel Doc XR+ system (BioRad) or Sapphire
587 Biomolecular Imager (Azure Biosystems) and analyzed with either Image Lab version 6.0.1 or
588 AzureSpot (Azure Biosystems).
589
590 **Single-cycle infectivity assays**. TZM-bl is a HeLa-derived cell line which contains a stably
591 integrated HIV-LTR-luciferase construct (73, 74). TZM-bl cells were infected with serial dilutions
592 of RT-normalized virus stock (44) in the presence of 10 μg/ml DEAE-dextran. For SARS-CoV-2
593 S infectivity assays, HEK293T cells stably expressing hACE2 (BEI resources, NR-52511) were
594 infected with serial dilutions of RT-normalized S-pseudotyped, luciferase-expressing HIV-1
595 (pNL4-3.Luc.R-E-) virus stock in the presence of 10 μg/ml DEAE-dextran. Cells were lysed with
596 BriteLite Luciferase reagent (Perkin-Elmer) and luciferase was measured in a Wallac BetaMax
597 Plate reader at 48 hours post-infection. Data were normalized to non-MARCH transfected
598 negative control from three independent experiments.
599
600 **Confocal microscopy**. Microscopy experiments used 18mm coverslips (Electron Microscopy
601 Sciences, catalog number 72291-06) which were sterilized by soaking in ethanol and air-dried
602 before seeding HEK293T cells onto them. Coverslips were pre-treated with fibronectin (Sigma-
603 Aldrich, #GC010) at 1:50 dilution in PBS for 30 min at room temperature before seeding cells.
604 HEK293T cells were cultured overnight and fixed with 4% paraformaldehyde (Electron
605 Microscopy Sciences, BM-155) at 24 hr post-transfection in DPBS for 1 hr, quenched with 0.1M

606 glycine in PBS for 10 min. Cells were permeabilized with 0.2% Triton X-100 (Sigma-Aldrich,
607 #T-8787) in PBS for 5 min, blocked with 10% BSA/PBS (Sigma-Aldrich) for 30 min and stained
608 with primary antibodies at a 1:400 dilution with 0.1% Triton and 1% BSA in PBS for 1 hr. After
609 3 washes in PBS, cells were incubated with secondary antibodies and DAPI stain in 1:1000 dilution
610 in PBS. Antibody information is listed in Table S2. Cells were washed and mounted with
611 Fluoromount-G (Electron Microscopy Sciences, #0100-01). Imaging was performed with a Leica
612 TCS SP8 microscope (Leica Microsystems Inc., Buffalo Grove, IL) using a 63X oil-immersion
613 objective. Images were generated using ImageJ software (NIH, Bethesda, MD). Background was
614 subtracted using imageJ's built-in 'rolling ball' background subtraction process. Colocalization
615 analyses were performed with intracellular region of interest (ROI) excluding any plasma-
616 membrane associated signal using Colocalization test and a Plugin, EzColocalization, (75) with
617 ImageJ. Cells were excluded from analysis if they were not transfected.
618
619 **RT-qPCR**. To measure *MARCH8* expression levels, total RNA was extracted using RNeasy Plus
620 Mini Kit (Qiagen) following manufacturer's instructions from transfected HEK293T, cell-lines or
621 cells stimulated with 1000U/ml of IFN- α, β or γ (Pblassay science, catalog number 11200, 11415
622 and 11500). RNA was transcribed using High-Capacity cDNA Reverse Transcription Kit
623 (Applied Biosystems) and real time PCR was performed using KAPA Sybr Fast master mix (Kapa
624 Biosystems) following manufacturer's instructions using CFX connect real-time PCR detection
625 system (BioRad) with specific oligonucleotides described previously (6, 11). The *MARCH8*
626 mRNA levels were normalized with *GAPDH* mRNA levels using ΔΔCT method for relative
627 quantification.
628
629 **siRNA knockdown of endogenous *MARCH8*.** HEK293T cells were transfected with 0.01, 0.1
630 and 1 μM MARCH8-specific siRNA or non-targeting control (NTC) (Smart pool, Dharmacon)
631 using Lipofectamine RNAiMAX (ThermoFisher Scientific) following the manufactuer's protocol.
632 Seventy-two hrs post siRNA treatment, cells were collected for RT-qPCR to measure *MARCH8*
633 expression. The siRNA-treated HEK293T cells were transfected with HIV-1 pNL4-3 clone, and
634 the progeny viruses were collected at 48 hr post transfection, RT normalized and used to infect
635 the TZM-bl indicator cell line.
636

Acknowledgements:
We thank following Kenzo Tokunaga, Alan Rein and Alex Compton for providing reagents. We thank Sherimay Ablan and Melissa V. Fernandez for technical advice and members of the Freed lab for critical review of the manuscript and helpful discussion. We thank Kim Peifley and David Scheiblin (NCI-Frederick) for technical advice.

Funding information

Research in the Freed lab is supported by the Intramural Research Program of the Center for Cancer Research, National Cancer Institute, National Institutes of Health. Funds were also provided by a grant from the Intramural Targeted Anti-COVID-19 (ITAC) Program and from an Intramural AIDS Research Fellowship (for CML).

Author contributions:
Designed research: CML, AW & EOF
Performed research: CML, AW, AM and NP
Analyzed data: CML & AW
Wrote paper: CML, AW and EOF

References:

1. Ghimire D, Rai M, Gaur R. 2018. Novel host restriction factors implicated in HIV-1 replication. J Gen Virol 99:435-446.
2. Forlani G, Shallak M, Ramia E, Tedeschi A, Accolla RS. 2019. Restriction factors in human retrovirus infections and the unprecedented case of CIITA as link of intrinsic and adaptive immunity against HTLV-1. Retrovirology 16:34.
3. Jia X, Zhao Q, Xiong Y. 2015. HIV suppression by host restriction factors and viral immune evasion. Curr Opin Struct Biol 31:106-14.
4. V DU, De Crignis E, Re MC. 2018. Host Restriction Factors and Human Immunodeficiency Virus (HIV-1): A Dynamic Interplay Involving All Phases of the Viral Life Cycle. Curr HIV Res 16:184-207.
5. Beitari S, Wang Y, Liu SL, Liang C. 2019. HIV-1 Envelope Glycoprotein at the Interface of Host Restriction and Virus Evasion. Viruses 11.
6. Zhang Y, Tada T, Ozono S, Yao W, Tanaka M, Yamaoka S, Kishigami S, Fujita H, Tokunaga K. 2019. Membrane-associated RING-CH (MARCH) 1 and 2 are MARCH family members that inhibit HIV-1 infection. J Biol Chem 294:3397-3405.
7. Braun E, Hotter D, Koepke L, Zech F, Gross R, Sparrer KMJ, Muller JA, Pfaller CK, Heusinger E, Wombacher R, Sutter K, Dittmer U, Winkler M, Simmons G, Jakobsen MR, Conzelmann KK, Pohlmann S, Munch J, Fackler OT, Kirchhoff F, Sauter D. 2019. Guanylate-Binding Proteins 2 and 5 Exert Broad Antiviral Activity by Inhibiting Furin-Mediated Processing of Viral Envelope Proteins. Cell Rep 27:2092-2104 e10.

680 8. Zhang Y, Lu J, Liu X. 2018. MARCH2 is upregulated in HIV-1 infection and inhibits HIV-1
681 production through envelope protein translocation or degradation. Virology 518:293-
682 300.
683 9. Hotter D, Sauter D, Kirchhoff F. 2017. Guanylate binding protein 5: Impairing virion
684 infectivity by targeting retroviral envelope glycoproteins. Small GTPases 8:31-37.
685 10. Krapp C, Hotter D, Gawanbacht A, McLaren PJ, Kluge SF, Sturzel CM, Mack K, Reith E,
686 Engelhart S, Ciuffi A, Hornung V, Sauter D, Telenti A, Kirchhoff F. 2016. Guanylate
687 Binding Protein (GBP) 5 Is an Interferon-Inducible Inhibitor of HIV-1 Infectivity. Cell Host
688 Microbe 19:504-14.
689 11. Tada T, Zhang Y, Koyama T, Tobiume M, Tsunetsugu-Yokota Y, Yamaoka S, Fujita H,
690 Tokunaga K. 2015. MARCH8 inhibits HIV-1 infection by reducing virion incorporation of
691 envelope glycoproteins. Nat Med 21:1502-7.
692 12. Sood C, Marin M, Chande A, Pizzato M, Melikyan GB. 2017. SERINC5 protein inhibits
693 HIV-1 fusion pore formation by promoting functional inactivation of envelope
694 glycoproteins. J Biol Chem 292:6014-6026.
695 13. Usami Y, Wu Y, Gottlinger HG. 2015. SERINC3 and SERINC5 restrict HIV-1 infectivity and
696 are counteracted by Nef. Nature 526:218-23.
697 14. Rey FA, Lok SM. 2018. Common Features of Enveloped Viruses and Implications for
698 Immunogen Design for Next-Generation Vaccines. Cell 172:1319-1334.
699 15. Tang T, Bidon M, Jaimes JA, Whittaker GR, Daniel S. 2020. Coronavirus membrane fusion
700 mechanism offers a potential target for antiviral development. Antiviral Res
701 178:104792.
702 16. Ghosh S, Dellibovi-Ragheb TA, Kerviel A, Pak E, Qiu Q, Fisher M, Takvorian PM, Bleck C,
703 Hsu VW, Fehr AR, Perlman S, Achar SR, Straus MR, Whittaker GR, de Haan CAM, Kehrl J,
704 Altan-Bonnet G, Altan-Bonnet N. 2020. beta-Coronaviruses Use Lysosomes for Egress
705 Instead of the Biosynthetic Secretory Pathway. Cell doi:10.1016/j.cell.2020.10.039.
706 17. Komander D, Rape M. 2012. The ubiquitin code. Annu Rev Biochem 81:203-29.
707 18. Bauer J, Bakke O, Morth JP. 2017. Overview of the membrane-associated RING-CH
708 (MARCH) E3 ligase family. N Biotechnol 38:7-15.
709 19. Bartee E, Mansouri M, Hovey Nerenberg BT, Gouveia K, Fruh K. 2004. Downregulation of
710 major histocompatibility complex class I by human ubiquitin ligases related to viral
711 immune evasion proteins. J Virol 78:1109-20.
712 20. Goto E, Ishido S, Sato Y, Ohgimoto S, Ohgimoto K, Nagano-Fujii M, Hotta H. 2003. c-MIR,
713 a human E3 ubiquitin ligase, is a functional homolog of herpesvirus proteins MIR1 and
714 MIR2 and has similar activity. J Biol Chem 278:14657-68.
715 21. Ishido S, Wang C, Lee BS, Cohen GB, Jung JU. 2000. Downregulation of major
716 histocompatibility complex class I molecules by Kaposi's sarcoma-associated herpesvirus
717 K3 and K5 proteins. J Virol 74:5300-9.
718 22. Coscoy L, Ganem D. 2000. Kaposi's sarcoma-associated herpesvirus encodes two
719 proteins that block cell surface display of MHC class I chains by enhancing their
720 endocytosis. Proc Natl Acad Sci U S A 97:8051-6.
721 23. Nash K, Chen W, Salganik M, Muzyczka N. 2009. Identification of cellular proteins that
722 interact with the adeno-associated virus rep protein. J Virol 83:454-69.

723 24. Oh J, Shin JS. 2015. Molecular mechanism and cellular function of MHCII ubiquitination.
724 Immunol Rev 266:134-44.
725 25. Fujita H, Iwabu Y, Tokunaga K, Tanaka Y. 2013. Membrane-associated RING-CH (MARCH)
726 8 mediates the ubiquitination and lysosomal degradation of the transferrin receptor. J
727 Cell Sci 126:2798-809.
728 26. van de Kooij B, Verbrugge I, de Vries E, Gijsen M, Montserrat V, Maas C, Neefjes J, Borst
729 J. 2013. Ubiquitination by the membrane-associated RING-CH-8 (MARCH-8) ligase
730 controls steady-state cell surface expression of tumor necrosis factor-related apoptosis
731 inducing ligand (TRAIL) receptor 1. J Biol Chem 288:6617-28.
732 27. Bartee E, Eyster CA, Viswanathan K, Mansouri M, Donaldson JG, Fruh K. 2010.
733 Membrane-Associated RING-CH proteins associate with Bap31 and target CD81 and
734 CD44 to lysosomes. PLoS One 5:e15132.
735 28. Chen R, Li M, Zhang Y, Zhou Q, Shu HB. 2012. The E3 ubiquitin ligase MARCH8 negatively
736 regulates IL-1beta-induced NF-kappaB activation by targeting the IL1RAP coreceptor for
737 ubiquitination and degradation. Proc Natl Acad Sci U S A 109:14128-33.
738 29. Eyster CA, Cole NB, Petersen S, Viswanathan K, Fruh K, Donaldson JG. 2011. MARCH
739 ubiquitin ligases alter the itinerary of clathrin-independent cargo from recycling to
740 degradation. Mol Biol Cell 22:3218-30.
741 30. Roy N, Pacini G, Berlioz-Torrent C, Janvier K. 2017. Characterization of E3 ligases
742 involved in lysosomal sorting of the HIV-1 restriction factor BST2. J Cell Sci 130:1596-
743 1611.
744 31. Hewitt EW, Duncan L, Mufti D, Baker J, Stevenson PG, Lehner PJ. 2002. Ubiquitylation of
745 MHC class I by the K3 viral protein signals internalization and TSG101-dependent
746 degradation. EMBO J 21:2418-29.
747 32. Mansouri M, Bartee E, Gouveia K, Hovey Nerenberg BT, Barrett J, Thomas L, Thomas G,
748 McFadden G, Fruh K. 2003. The PHD/LAP-domain protein M153R of myxomavirus is a
749 ubiquitin ligase that induces the rapid internalization and lysosomal destruction of CD4.
750 J Virol 77:1427-40.
751 33. Coscoy L, Ganem D. 2001. A viral protein that selectively downregulates ICAM-1 and B7-
752 2 and modulates T cell costimulation. J Clin Invest 107:1599-606.
753 34. Boname JM, Stevenson PG. 2001. MHC class I ubiquitination by a viral PHD/LAP finger
754 protein. Immunity 15:627-36.
755 35. Cadwell K, Coscoy L. 2005. Ubiquitination on nonlysine residues by a viral E3 ubiquitin
756 ligase. Science 309:127-30.
757 36. Cadwell K, Coscoy L. 2008. The specificities of Kaposi's sarcoma-associated herpesvirus-
758 encoded E3 ubiquitin ligases are determined by the positions of lysine or cysteine
759 residues within the intracytoplasmic domains of their targets. J Virol 82:4184-9.
760 37. Wang X, Herr RA, Chua WJ, Lybarger L, Wiertz EJ, Hansen TH. 2007. Ubiquitination of
761 serine, threonine, or lysine residues on the cytoplasmic tail can induce ERAD of MHC-I
762 by viral E3 ligase mK3. J Cell Biol 177:613-24.
763 38. Liu L, Oliveira NM, Cheney KM, Pade C, Dreja H, Bergin AM, Borgdorff V, Beach DH,
764 Bishop CL, Dittmar MT, McKnight A. 2011. A whole genome screen for HIV restriction
765 factors. Retrovirology 8:94.

766 39. Volchkov VE, Feldmann H, Volchkova VA, Klenk HD. 1998. Processing of the Ebola virus
767 glycoprotein by the proprotein convertase furin. Proc Natl Acad Sci U S A 95:5762-7.
768 40. Coutard B, Valle C, de Lamballerie X, Canard B, Seidah NG, Decroly E. 2020. The spike
769 glycoprotein of the new coronavirus 2019-nCoV contains a furin-like cleavage site
770 absent in CoV of the same clade. Antiviral Res 176:104742.
771 41. Checkley MA, Luttge BG, Freed EO. 2011. HIV-1 envelope glycoprotein biosynthesis,
772 trafficking, and incorporation. J Mol Biol 410:582-608.
773 42. Freed EO, Martin MA. 1995. The role of human immunodeficiency virus type 1 envelope
774 glycoproteins in virus infection. J Biol Chem 270:23883-6.
775 43. Freed EO, Martin MA. 1996. Domains of the human immunodeficiency virus type 1
776 matrix and gp41 cytoplasmic tail required for envelope incorporation into virions. J Virol
777 70:341-51.
778 44. Willey RL, Smith DH, Lasky LA, Theodore TS, Earl PL, Moss B, Capon DJ, Martin MA. 1988.
779 In vitro mutagenesis identifies a region within the envelope gene of the human
780 immunodeficiency virus that is critical for infectivity. J Virol 62:139-47.
781 45. Dodd RB, Allen MD, Brown SE, Sanderson CM, Duncan LM, Lehner PJ, Bycroft M, Read
782 RJ. 2004. Solution structure of the Kaposi's sarcoma-associated herpesvirus K3 N-
783 terminal domain reveals a Novel E2-binding C4HC3-type RING domain. J Biol Chem
784 279:53840-7.
785 46. Jabbour M, Campbell EM, Fares H, Lybarger L. 2009. Discrete Domains of MARCH1
786 Mediate Its Localization, Functional Interactions, and Posttranscriptional Control of
787 Expression. The Journal of Immunology 183:6500-6512.
788 47. Tran EE, Simmons JA, Bartesaghi A, Shoemaker CJ, Nelson E, White JM, Subramaniam S.
789 2014. Spatial localization of the Ebola virus glycoprotein mucin-like domain determined
790 by cryo-electron tomography. J Virol 88:10958-62.
791 48. Ou X, Liu Y, Lei X, Li P, Mi D, Ren L, Guo L, Guo R, Chen T, Hu J, Xiang Z, Mu Z, Chen X,
792 Chen J, Hu K, Jin Q, Wang J, Qian Z. 2020. Characterization of spike glycoprotein of SARS-
793 CoV-2 on virus entry and its immune cross-reactivity with SARS-CoV. Nat Commun
794 11:1620.
795 49. Ujike M, Huang C, Shirato K, Makino S, Taguchi F. 2016. The contribution of the
796 cytoplasmic retrieval signal of severe acute respiratory syndrome coronavirus to
797 intracellular accumulation of S proteins and incorporation of S protein into virus-like
798 particles. J Gen Virol 97:1853-1864.
799 50. Lontok E, Corse E, Machamer CE. 2004. Intracellular targeting signals contribute to
800 localization of coronavirus spike proteins near the virus assembly site. J Virol 78:5913-
801 22.
802 51. Samji T, Hong S, Means RE. 2014. The Membrane Associated RING-CH Proteins: A Family
803 of E3 Ligases with Diverse Roles through the Cell. International Scholarly Research
804 Notices 2014:637295.
805 52. Schneider WM, Chevillotte MD, Rice CM. 2014. Interferon-stimulated genes: a complex
806 web of host defenses. Annu Rev Immunol 32:513-45.
807 53. Colomer-Lluch M, Ruiz A, Moris A, Prado JG. 2018. Restriction Factors: From Intrinsic
808 Viral Restriction to Shaping Cellular Immunity Against HIV-1. Front Immunol 9:2876.

809 54. Schoggins JW, Rice CM. 2011. Interferon-stimulated genes and their antiviral effector
810 functions. Curr Opin Virol 1:519-25.
811 55. Zhang Y, Tada T, Ozono S, Kishigami S, Fujita H, Tokunaga K. 2020. MARCH8 inhibits viral
812 infection by two different mechanisms. Elife 9.
813 56. Nakamura N, Fukuda H, Kato A, Hirose S. 2005. MARCH-II is a syntaxin-6-binding protein
814 involved in endosomal trafficking. Mol Biol Cell 16:1696-710.
815 57. Nakamura N. 2011. The Role of the Transmembrane RING Finger Proteins in Cellular and
816 Organelle Function. Membranes (Basel) 1:354-93.
817 58. Herr RA, Harris J, Fang S, Wang X, Hansen TH. 2009. Role of the RING-CH domain of viral
818 ligase mK3 in ubiquitination of non-lysine and lysine MHC I residues. Traffic 10:1301-17.
819 59. Yu C, Li S, Zhang X, Khan I, Ahmad I, Zhou Y, Li S, Shi J, Wang Y, Zheng YH. 2020. MARCH8
820 Inhibits Ebola Virus Glycoprotein, Human Immunodeficiency Virus Type 1 Envelope
821 Glycoprotein, and Avian Influenza Virus H5N1 Hemagglutinin Maturation. mBio 11.
822 60. Freed EO, Martin MA. 2013. Human Immunodeficiency Viruses: Replication, p 1502-
823 2456. *In* Knipe DM, Howley P (ed), Fields Virology, 6 ed. Wolters Kluwer, Philadelphia.
824 61. Feldmann H, Sanchez AS, Geisbert TW. 2013. Filoviridae: Marburg and Ebola Viruses, p
825 923-2456. *In* Knipe DM, Howley P (ed), Fields Virology, 6 ed. Wolters Kluwer,
826 Philadelphia.
827 62. Masters PS, Perlman S. 2013. Coronaviridae, p 825-2456. *In* Knipe DM, Howley P (ed),
828 Fields Virology, 6 ed. Wolters Kluwer, Philadelphia.
829 63. Lyles DS, Kuzmin IV, Rupprecht CE. 2013. Rhabdoviridae, p 885-2456. *In* Knipe DM,
830 Howley P (ed), Fields Virology, 6 ed. Wolters Kluwer, Philadelphia.
831 64. Sa Ribero M, Jouvenet N, Dreux M, Nisole S. 2020. Interplay between SARS-CoV-2 and
832 the type I interferon response. PLoS Pathog 16:e1008737.
833 65. Acosta PL, Byrne AB, Hijano DR, Talarico LB. 2020. Human Type I Interferon Antiviral
834 Effects in Respiratory and Reemerging Viral Infections. Journal of Immunology Research
835 2020:1372494.
836 66. Zhang Q, Bastard P, Liu Z, Le Pen J, Moncada-Velez M, Chen J, Ogishi M, Sabli IKD,
837 Hodeib S, Korol C, Rosain J, Bilguvar K, Ye J, Bolze A, Bigio B, Yang R, Arias AA, Zhou Q,
838 Zhang Y, Onodi F, Korniotis S, Karpf L, Philippot Q, Chbihi M, Bonnet-Madin L, Dorgham
839 K, Smith N, Schneider WM, Razooky BS, Hoffmann HH, Michailidis E, Moens L, Han JE,
840 Lorenzo L, Bizien L, Meade P, Neehus AL, Ugurbil AC, Corneau A, Kerner G, Zhang P,
841 Rapaport F, Seeleuthner Y, Manry J, Masson C, Schmitt Y, Schluter A, Le Voyer T, Khan T,
842 Li J, et al. 2020. Inborn errors of type I IFN immunity in patients with life-threatening
843 COVID-19. Science 370.
844 67. Gale M, Jr., Sen GC. 2009. Viral evasion of the interferon system. J Interferon Cytokine
845 Res 29:475-6.
846 68. Murakami T, Freed EO. 2000. The long cytoplasmic tail of gp41 is required in a cell type-
847 dependent manner for HIV-1 envelope glycoprotein incorporation into virions.
848 Proceedings of the National Academy of Sciences 97:343-348.
849 69. Freed EO, Martin MA. 1995. Virion incorporation of envelope glycoproteins with long
850 but not short cytoplasmic tails is blocked by specific, single amino acid substitutions in
851 the human immunodeficiency virus type 1 matrix. J Virol 69:1984-9.

852 70. Yee JK, Friedmann T, Burns JC. 1994. Generation of high-titer pseudotyped retroviral
853 vectors with very broad host range. Methods Cell Biol 43 Pt A:99-112.
854 71. Burns JC, Friedmann T, Driever W, Burrascano M, Yee JK. 1993. Vesicular stomatitis virus
855 G glycoprotein pseudotyped retroviral vectors: concentration to very high titer and
856 efficient gene transfer into mammalian and nonmammalian cells. Proc Natl Acad Sci U S
857 A 90:8033-7.
858 72. Sherer NM, Lehmann MJ, Jimenez-Soto LF, Ingmundson A, Horner SM, Cicchetti G, Allen
859 PG, Pypaert M, Cunningham JM, Mothes W. 2003. Visualization of retroviral replication
860 in living cells reveals budding into multivesicular bodies. Traffic 4:785-801.
861 73. Platt EJ, Wehrly K, Kuhmann SE, Chesebro B, Kabat D. 1998. Effects of CCR5 and CD4 Cell
862 Surface Concentrations on Infections by Macrophagetropic Isolates of Human
863 Immunodeficiency Virus Type 1. Journal of Virology 72:2855-2864.
864 74. Wei X, Decker JM, Liu H, Zhang Z, Arani RB, Kilby JM, Saag MS, Wu X, Shaw GM, Kappes
865 JC. 2002. Emergence of Resistant Human Immunodeficiency Virus Type 1 in Patients
866 Receiving Fusion Inhibitor (T-20) Monotherapy. Antimicrobial Agents and Chemotherapy
867 46:1896-1905.
868 75. Stauffer W, Sheng H, Lim HN. 2018. EzColocalization: An ImageJ plugin for visualizing
869 and measuring colocalization in cells and organisms. Sci Rep 8:15764.
870

871 **Figure legends**

872 **Figure 1. Organization of the viral envelope glycoproteins used in this study.** Surface and
873 transmembrane subunits of HIV-1 Env (gp120 and gp41), EboV-GP (GP1 and GP2) and SARS-
874 CoV-2 S protein (S1 and S2) are indicated. Where appropriate, the site of furin cleavage is
875 indicated by the red arrow. The Δmucin-like domain (ΔMLD, dotted rectangle with hatching
876 mark) and the receptor-binding domain (RBD) of the EboV-GP and SARS-CoV-2 S protein,
877 respectively, are indicated. The fusion peptide (FP) and transmembrane domains (TM) are labeled.
878 The length in amino acids (aa) of each full-length (FL) CT, and the number of Lys (K) residues in
879 each CT, are indicated. Each CT mutant, and the Lys residues mutated to either Arg (R) or Ala
880 (A), are shown. At the bottom is shown a schematic representation of the MARCH8 topology in
881 the membrane, with two transmembrane domains and the RING finger E3 ligase domain. The
882 structures of the viral glycoproteins and MARCH8 are not drawn to scale.

883

884 **Figure 2. MARCH8-mediated targeting of viral envelope glycoproteins exhibits differential**
885 **dependence on the CT. (A)** HEK293T cells in a 12-well plate were cotransfected with the Env-
886 defective HIV-1 molecular clone pNL4-3/KFS (1 μg) and vectors expressing WT or mutant VSV-
887 G (100 ng) and HA-tagged WT or mutant MARCH8 (50 ng). TZM-bl cells were infected with
888 VSV-G pseudotyped HIV-1 and luciferase activity was measured two days post-infection and
889 normalized for viral p24. Infectivity of particles pseudotyped with WT VSV-G in the absence of
890 MARCH8 is set to 100%. **(B)** HEK293T cells were cotransfected with WT or CT-deleted
891 (CTdel144) pNL4-3 HIV-1 molecular clones (1 μg), and vectors expressing HA-tagged MARCH8
892 (WT or mutants) (100 ng). Two days posttransfection, virus supernatants were collected, analyzed
893 for p24 content by western blot, and infections were carried out in TZM-bl cells, and normalized
894 to p24 as described in **(A)**. Infectivity of WT HIV-1 in the absence of MARCH8 was set to 100%.
895 **(C)** HEK293T cells were cotransfected with Env-defective (pNL4-3/KFS) HIV-1 molecular clone
896 (1 μg), and vectors expressing EboV-GP (WT or CT mutants) (500 ng) and HA-tagged MARCH8
897 (WT or mutants) (250 ng), and infections were carried out in TZM-bl cells. Infectivity of particles
898 pseudotyped with WT EboV-GP in the absence of MARCH8 was set to 100%. **D)** HEK293T cells
899 in a 6-well plate were cotransfected with the Env-defective, luciferase-expressing pNL4-3
900 derivative pNL4-3.Luc.R-E- (3 μg) and vectors expressing SARS-CoV-2-S full-length (FL) and
901 mutants (FL-K-to-R, Truncated, Truncated-K-to-R) (300 ng) and HA-tagged MARCH8 (WT or

902 CS mutant) (200 ng). Two days post-transfection, virus supernatant was collected, and infectivity
903 was measured in HEK293T cells stably expressing hACE2 with RT-normalized virus. Infectivity
904 of virus particles pseudotyped with FL S protein in the absence of MARCH8 was set to 100%.
905 Data shown are ± SD from 3-5 independent experiments. P values (two-tailed unpaired t-test): *p
906 < 0.05, **p < 0.01, ****p < 0.0001.
907
908 **Figure 3. Effect of MARCH8 on virion incorporation of VSV-G is CT dependent. (A)**
909 HEK293T cells were cotransfected with the Env-defective HIV-1 molecular clone pNL4-3/KFS
910 (1 μg), and vectors expressing WT or mutant VSV-G (100 ng), HA-tagged WT or mutant
911 MARCH8 (50 ng) and FLAG-tagged SGTA (200 ng) as a transfection control. Cell and viral
912 lysates were prepared and subjected to western blot analysis with anti-VSV-G to detect VSV-G;
913 HIV-Ig to detect the Gag proteins Pr55Gag and p24 (CA); anti-HA to detect HA-tagged
914 MARCH8; or anti-FLAG to detect FLAG-tagged SGTA. Mobility of molecular mass standards is
915 shown on the right of each blot. **(B)** The levels of VSV-G in cell and virus was quantified, and the
916 levels of VSV-G in virus was normalized to viral p24. The levels of VSV-G in the absence of
917 MARCH8 was set to 100%. **(C)** HEK293T cells were transfected with VSV-G expression vector
918 in the absence or presence of HA-tagged MARCH8 expression vector. One day post-transfection,
919 cells were labeled with [^{35}S]Met/Cys for 20 min and then chased for 0, 2, or 4 h in unlabeled
920 medium. Cell lysates were prepared and immunoprecipitated with anti-VSV-G Ab and analyzed
921 by SDS-PAGE followed by fluorography. The levels of VSV-G were quantified, and set to 100%
922 at time zero. Data shown are ± SD from 4-5 **(B)** or 2 **(C)** independent experiments. P values (two-
923 tailed unpaired t-test): *p < 0.05, **p < 0.02, ***p < 0.01, ****p < 0.0001.
924
925 **Figure 4. Effect of MARCH8 on HIV-1 Env processing and incorporation is CT independent.**
926 **(A)** HEK293T cells were cotransfected with pNL4-3 or pNL4-3/CTdel144 molecular clones (1
927 μg) in the absence or presence of vectors expressing HA-tagged WT or mutant MARCH8 (100
928 ng) and FLAG-tagged SGTA as a transfection control. Two days post-transfection, cell and viral
929 lysates were prepared and subjected to western blot analysis with anti-Env to detect gp160, gp120
930 and gp41; HIV-Ig to detect Gag proteins, Pr55Gag and p24 (CA); anti-HA to detect HA-tagged
931 MARCH8; or anti-FLAG to detect FLAG-tagged SGTA. Mobility of molecular mass standards is
932 shown on the right of the blots. **(B)** The levels of gp120 in virus was quantified and normalized to

933 p24, and set to 100% in the absence of MARCH8. **(C)** The levels of gp41 in virus was quantified
934 and normalized to p24, and set to 100% in the absence of MARCH8. Data shown are ± SD from
935 three independent experiments. P values (two-tailed unpaired t-test): ***p < 0.001, ****p <
936 0.0001.
937
938 **Figure 5. Effect of MARCH8 on processing and virion incorporation of EboV-GP is CT**
939 **independent. (A)** HEK293T cells were cotransfected with the Env-defective HIV-1 molecular
940 clone pNL4-3/KFS (1 μg) with vectors expressing WT or mutant EboV-GP (500 ng), HA-tagged
941 WT or mutant MARCH8 (250 ng) and FLAG-tagged SGTA as a transfection control. Two days
942 post-transfection, cell and viral lysates were prepared and subjected to western blot analysis with
943 anti-EboV-GP Abs to detect Pre-GP (G0), GP1, and GP2, HIV-Ig to detect Gag proteins, anti-HA
944 to detect HA-tagged MARCH8 or anti-FLAG to detect FLAG-tagged SGTA. Mobility of
945 molecular mass standards is shown on the right of the blots. **(B)** The levels of GP0+GP1 and GP2
946 in the cell were quantified, and the levels in the absence of MARCH8 were set to 100%. **(C)** The
947 levels of GP0+GP1 and GP2 in virus were quantified and normalized to p24, and set to 100% in
948 the absence of MARCH8. **(D)** The processing of EboV-GP in cells was quantified by calculating
949 the ratio of GP1/GP0, and set to 100% for the no MARCH8 control. Data shown are ± SD from
950 three independent experiments. P values (two-tailed unpaired t-test): *p < 0.05, **p < 0.01, ***p
951 < 0.001, ****p < 0.0001.
952
953 **Figure 6. Effect of MARCH8 on processing and virion incorporation of SARS-CoV-2-S is**
954 **CT independent. (A)** HEK293T were cotransfected with the Env-defective, luciferase-expressing
955 pNL4-3 derivative pNL4-3.Luc.R-E- (3 μg) with vectors expressing WT or mutant SARS-CoV-
956 2 S protein (300 ng), and WT or mutant HA-tagged MARCH8 (200 ng). Two days post-
957 transfection, cell and virus lysate were prepared and subjected to western blot analysis with anti-
958 SARS-CoV-2 S2 Ab to detect precursor S and S2; HIV-Ig to detect Gag proteins, Pr55Gag and
959 p24; and anti-HA to detect HA-tagged MARCH8. Molecular mass standards are shown on the
960 right of the blots. Red arrow indicates a putative less-glycosylated form SARS-CoV-2 S2 protein
961 in the cell lysate. **(B)** The level of SARS-CoV-2 S protein in cells was quantified and normalized
962 to p24; values were set to 100% in the absence of MARCH8. **(C)** The level of S2 was quantified
963 and normalized to p24 in virus; values were set to 100% in the absence of MARCH8. Data shown

964 are ± SD from three independent experiments. P values (two-tailed unpaired t-test): ***p < 0.001,
965 ****p < 0.0001.
966
967
968 **Figure 7. Knockdown of endogenous MARCH8 in HEK293T cells increases HIV-1**
969 **infectivity.** A) HEK293T cells were treated for 72 hrs with the indicated concentrations of
970 MARCH8-specific siRNA or a non-targeting control (NTC). Endogenous *MARCH8* RNA
971 expression was measured using RT-qPCR. B) siRNA-treated HEK293T cells in a 6-well plate
972 were transfected with the pNL4-3 HIV-1 molecular clone (3 μg). Two days posttransfection, virus
973 supernatants were collected, RT normalized, and used to infect TZM-bl cells. Infectivity in non-
974 siRNA-treated cells is set to 100%. Data shown are ± SD from 3 independent experiments. P
975 values (two-tailed unpaired t-test): *p < 0.05, **p < 0.01.
976
977 **Figure 8. Endogenous *MARCH8* gene expression is rapidly induced by IFN.** A) Endogenous
978 *MARCH8* RNA expression in the SupT1 T-cell line **(A)**, hPBMCs from 4 donors **(B)** and primary
979 human airway epithelial cells **(C)** and **D**) HEK293T cell line at 0, 0.5, 1, 2, and 4 hrs post-
980 stimulation with 1000U/ml type I (α and *β*) and II (γ) IFN. **E**) *MARCH8* expression in transfected
981 HEK293T cells after 48 hr post transfection (hpt) with increasing concentrations of MARCH8 (0,
982 50, 100 ng) in a 6-well tissue culture plate. Isolated RNA was subjected to RT-qPCR protocol as
983 detailed in the Materials and Methods. Fold increase in *MARCH8* RNA expression is normalized
984 to *GAPDH* expression levels. Data shown are ± SD from three independent experiments.
985
986 **Figure 9. MARCH8 traps WT VSV-G but not the VSV-G CT mutants in an intracellular**
987 **LAMP-1$^+$ compartment.** HEK293T cells were co-transfected with vectors expressing WT or
988 mutant VSV-G (200 ng) with or without vectors expressing HA-tagged MARCH8, MARCH8-CS
989 (100 ng) and the LAMP1-RFP or pDsRed-Golgi-Beta 1,4-galactosyltransferase (Golgi-
990 transferase) (300 ng) expression vectors. One day post-transfection cells, were processed for
991 confocal microscopy. Distribution of WT VSV-G **(A)**, VSV-G Tailless **(B)**, or VSV-G K-to-R
992 **(C)** in the absence or presence of WT MARCH8 or MARCH8-CS. Colocalization of VSV-G or
993 VSV-G mutants with WT MARCH8 **(D)** or MARCH8-CS **(E)** with the LAMP1-RFP or pDsRed-
994 Golgi-Beta 1,4-galactosyltransferase cellular markers. Scale bar = 10 μm.

995

996 **Figure 10. MARCH8 traps WT and truncated HIV-1 Env in an intracellular LAMP-1$^+$**
997 **compartment.** HEK293T cells were cotransfected with vectors expressing WT or truncated HIV-
998 1 Env (pIIINL4-Env or pIIINL4-EnvCTdel144, respectively) (200 ng), pSV-Tat, and HA-tagged
999 MARCH8 expression vectors (100 ng) and the LAMP1-RFP or pDsRed-Golgi-Beta 1,4-
1000 galactosyltransferase (300 ng) expression vectors. One day post-transfection cells were processed
1001 for confocal microscopy. Distribution of WT HIV-1 Env **(A)**, and EnvCTdel144 **(B)** in the absence
1002 or presence of WT MARCH8 or MARCH8-CS. Colocalization of HIV-1 Env and EnvCTdel144
1003 with MARCH8 **(C)** and MARCH-CS **(D)** and the LAMP1-RFP or pDsRed-Golgi-Beta 1,4-
1004 galactosyltransferase cellular markers. Scale bars = 10 µm.
1005

1006 **Figure 11. MARCH8 traps WT and truncated EboV-GP in an intracellular LAMP-1$^+$**
1007 **compartment**. HEK293T cells were cotransfected with vectors expressing EboV-GP or EboV-
1008 GP Tailless (200 ng) and HA-tagged MARCH8 expression vectors (100 ng) and the LAMP1-RFP
1009 or pDsRed-Golgi-Beta 1,4-galactosyltransferase (300 ng) expression vectors. One day post-
1010 transfection cells were processed for confocal microscopy. Distribution of EboV-GP **(A)** and
1011 EboV-GP Tailless **(B)** in the absence or presence of WT MARCH8 or MARCH8-CS.
1012 Colocalization of EboV-GP and EboV-GP Tailless with MARCH8 **(C)** and MARCH8-CS **(D)** and
1013 the LAMP1-RFP or pDsRed-Golgi-Beta 1,4-galactosyltransferase cellular markers. Scale bars =
1014 10 µm.
1015

1016 **Figure 12. MARCH8 traps WT and CT-mutant SARS-CoV-2 S proteins in an intracellular**
1017 **LAMP-1$^+$ compartment.** HEK293T cells were cotransfected with vectors expressing WT or CT-
1018 mutant SARS-CoV-2 S proteins (200 ng) and HA-tagged MARCH8 expression vectors (100 ng)
1019 and the LAMP1-RFP or pDsRed-Golgi-Beta 1,4-galactosyltransferase (300 ng) expression
1020 vectors. One day post-transfection cells were processed for confocal microscopy. Distribution of
1021 SARS-CoV-2 S-FL **(A)**, SARS-CoV-2 S-FL-K-to-R **(B)**, and SARS-CoV-2 S-Trun **(C)** and
1022 SARS-CoV-2 S-Trun-K-to-R **(D)** in the presence of MARCH8 and MARCH8-CS. Colocalization
1023 of SARS-CoV-2 S and CT mutants with MARCH8 **(E)** and MARCH8-CS **(F)** and the LAMP1-
1024 RFP or pDsRed-Golgi-Beta 1,4-galactosyltransferase cellular markers. Scale bars = 10 µm.
1025

1026 **Figure S1. MARCH8 is localized in the endolysosomal compartments and at the plasma**
1027 **membrane.** HEK293T cells were cotransfected with MARCH8 expression vector (200 ng) and
1028 the LAMP1-RFP or pDsRed-Golgi-Beta 1,4-galactosyltransferase (300 ng) expression vectors.
1029 Cells were fixed, processed and stained with anti-HA to detect MARCH8. Scale bars = 10 μm.
1030 Images were acquired with a Leica TCS SP8 confocal microscope. Colocalization between
1031 MARCH8 and subcellular compartment markers was assessed by calculating the Pearson's
1032 correlation coefficient (r values) ± SD using 50 cells per condition.
1033
1034 **Fig S2. Incorporation efficiency of viral glycoproteins into HIV-1 particles.** HEK293T cells
1035 were transfected with the WT (pNL4-3) or cotransfected with the Env-defective (pNL4-3/KFS)
1036 HIV-1 molecular clone and vectors expressing VSV-G or EboV-GP proteins or the Env-defective,
1037 luciferase-expressing pNL4-3 derivative pNL4-3.Luc.R-E- and a vector expressing the SARS-
1038 CoV-2 S protein. Two days post-transfection, cell and viral lysates were prepared and subjected
1039 to western blot analysis with antibodies against gp41, VSV-G, EboV GP2, or SARS-CoV-2 S2.
1040 The levels of viral glycoprotein in cell and virus lysates were quantified and incorporation
1041 efficiency was calculated as the amount of virion-associated glycoprotein relative to total
1042 glycoprotein in cell and virus. Data shown are + SD from three independent experiments. Plasmid
1043 concentrations indicated in legends of Fig 3-6.
1044
1045
1046
1047
1048
1049
1050
1051
1052
1053
1054

1055

Table 1. Colocalization of WT and mutant MARCH8, viral glycoproteins, and cellular markers

				+MARCH8		+MARCH8-CS	
		MARCH8	**MARCH8-CS**	**Golgi-transferase** [a]	**LAMP-1**	**Golgi-transferase**	**LAMP-1**
Viral GP[c]	VSV-G	0.92 ± 0.08 [b]	0.82 ± 0.13	0.91 ± 0.03	0.89 ± 0.06	0.88 ± 0.01	0.16 ± 0.01
	VSV-G Tailless	0.85 ± 0.11	0.80 ± 0.09	0.74 ± 0.14	0.31 ± 0.01	0.79 ± 0.15	0.18 ± 0.15
	VSV-G K-to-R	0.83 ± 0.01	0.79 ± 0.01	0.90 ± 0.02	0.32 ± 0.04	0.85 ± 0.04	0.14 ± 0.04
	HIV-1 Env	0.89 ± 0.13	0.79 ± 0.05	0.86 ± 0.07	0.79 ± 0.04	0.78 ± 0.02	0.18 ± 0.12
	HIV-1 EnvCTdel144	0.87 ± 0.12	0.79 ± 0.02	0.79 ± 0.16	0.76 ± 0.04	0.79 ± 0.11	0.19 ± 0.02
	EboV-GP	0.78 ± 0.06	0.73 ± 0.12	0.87 ± 0.11	0.67 ± 0.06	0.82 ± 0.08	0.12 ± 0.01
	EboV-GP Tailless	0.82 ± 0.08	0.71 ± 0.15	0.81 ± 0.07	0.61 ± 0.21	0.79 ± 0.16	0.15 ± 0.13
	SARS-CoV-2 S-FL	0.81 ± 0.01	0.72 ± 0.01	0.68 ± 0.13	0.65 ± 0.16	0.67 ± 0.08	0.20 ± 0.05
	SARS-CoV-2 S-FL-K-to-R	0.86 ± 0.11	0.77 ± 0.05	0.67 ± 0.14	0.67 ± 0.21	0.69 ± 0.12	0.18 ± 0.06
	SARS-CoV-2 S-Trun	0.89 ± 0.12	0.83 ± 0.03	0.79 ± 0.08	0.85 ± 0.08	0.78 ± 0.06	0.22 ± 0.14
	SARS-CoV-2 S-Trun K-to-R	0.92 ± 0.06	0.86 ± 0.13	0.81 ± 0.1	0.81 ± 0.16	0.80 ± 0.21	0.14 ± 0.01

1056

[a] Golgi-transferase = Beta 1,4-galatosyltransferase

[b] Pearson correlation coefficient (r) values, ± standard deviation (SD) using 50 cells per experimental condition. R-values indicate colocalization between MARCH8 and intracellular viral glycoprotein (first two columns), intracellular viral glycoprotein and cellular markers in the presence of WT MARCH8 (two middle columns), and intracellular viral glycoprotein and cellular markers in the presence of MARCH8-CS (right two columns)

[c] Viral glycoprotein

Figure 1

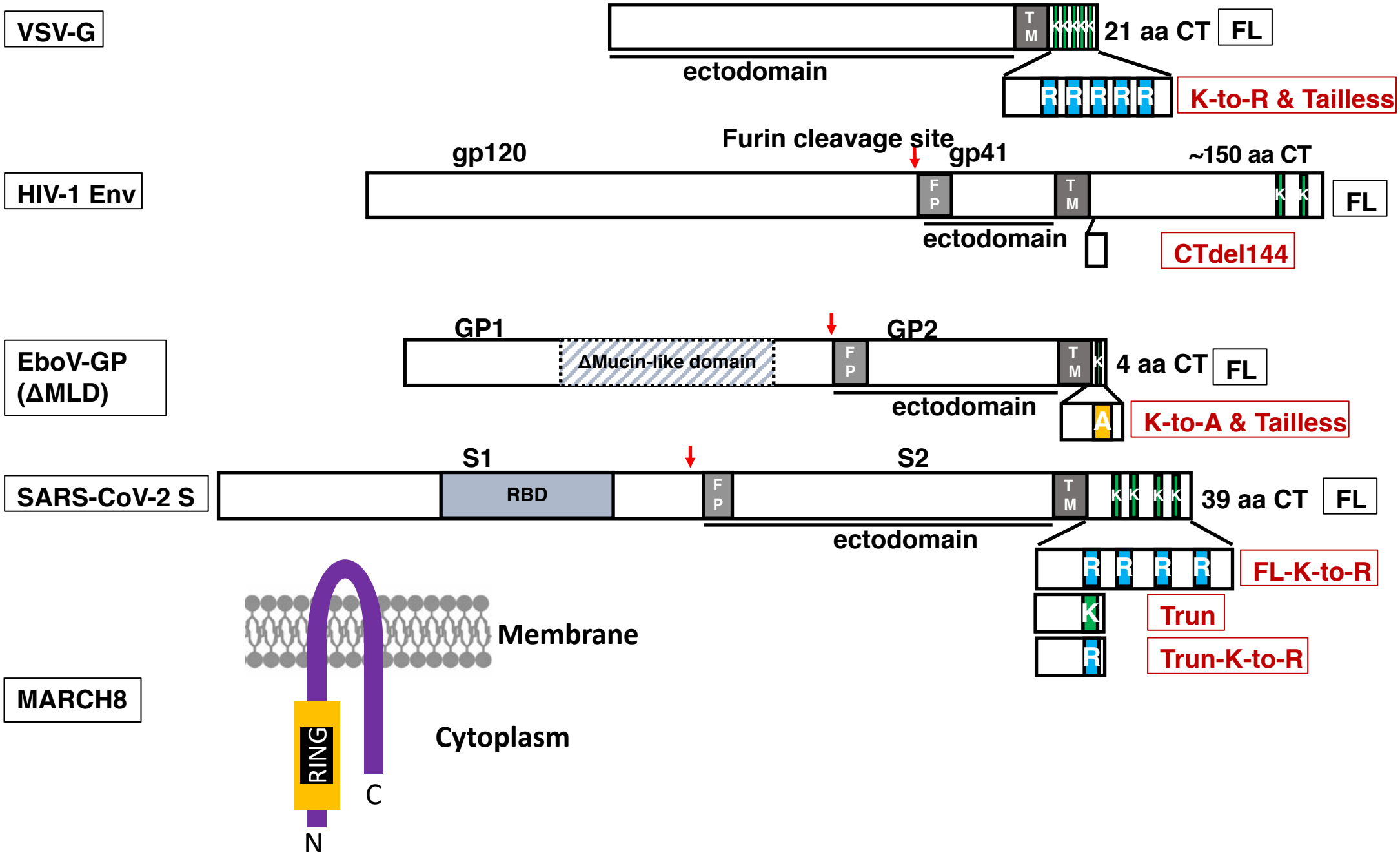
VSV-G
TM
KKKKKK
21 aa CT
FL
ectodomain
RRRRR
K-to-R & Tailless
HIV-1 Env
gp120
Furin cleavage site
gp41
~150 aa CT
FP
TM
KK
FL
ectodomain
CTdel144
EboV-GP
(ΔMLD)
GP1
GP2
ΔMucin-like domain
FP
TM
K
4 aa CT
FL
ectodomain
A
K-to-A & Tailless
SARS-CoV-2 S
S1
S2
RBD
FP
TM
KKKKK
39 aa CT
FL
ectodomain
RRRR
FL-K-to-R
K
Trun
R
Trun-K-to-R
MARCH8
Membrane
Cytoplasm
RING
C
N

Figure 2

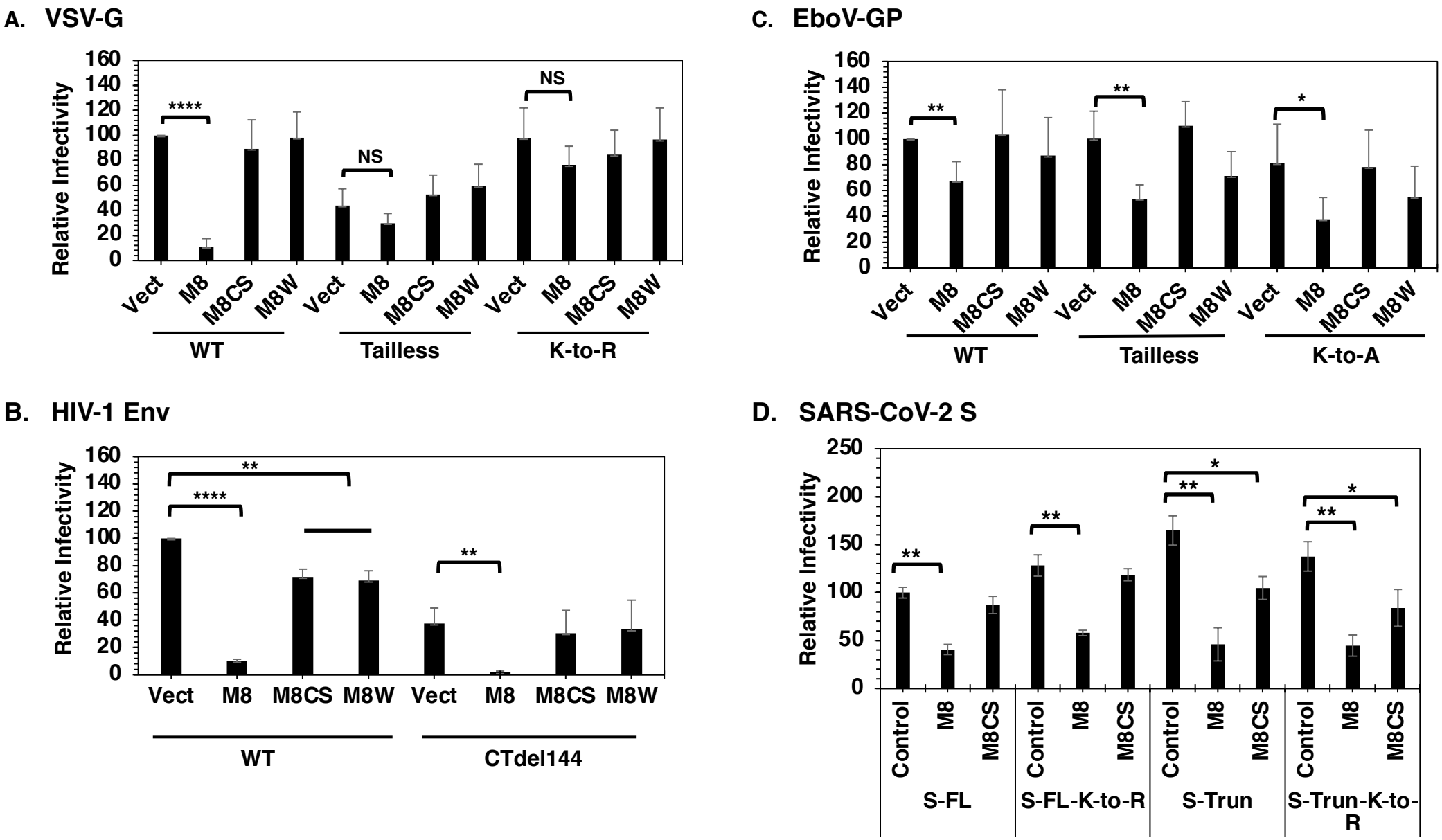
A. VSV-G
Relative Infectivity
160
140
120
100
80
60
40
20
0
****
NS
NS
Vect
M8
M8CS
M8W
WT
Tailless
K-to-R
B. HIV-1 Env
**
****
**
WT
CTdel144
C. EboV-GP
**
**
*
K-to-A
D. SARS-CoV-2 S
250
200
150
100
50
Control
S-FL
S-FL-K-to-R
S-Trun
S-Trun-K-to-R

Figure 3

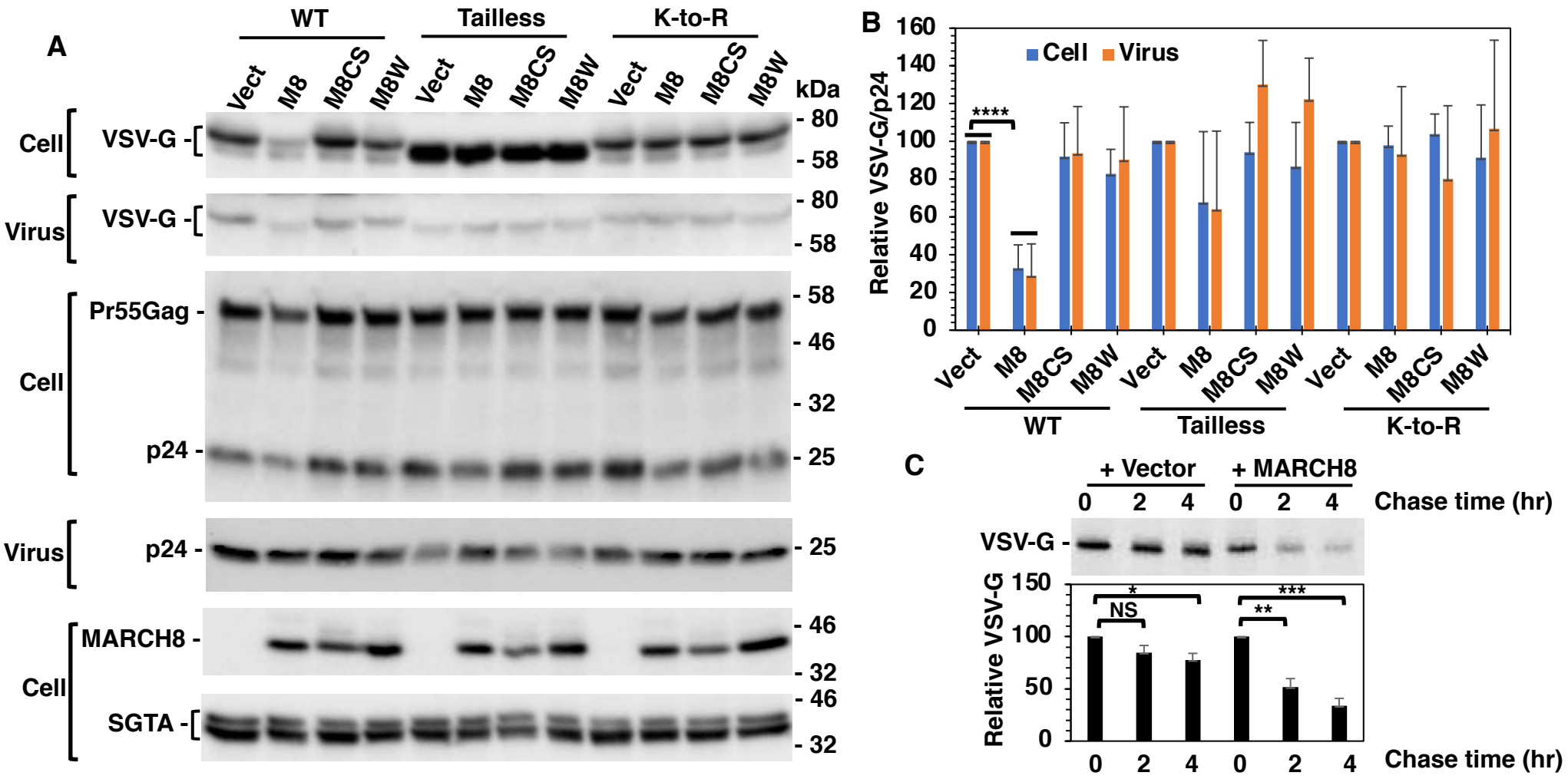
A
WT
Tailless
K-to-R
Vect
M8
M8CS
M8W
kDa
Cell
VSV-G
Virus
Pr55Gag
p24
MARCH8
SGTA
80
58
46
32
25
B
Cell
Virus
Relative VSV-G/p24
****
160
140
120
100
80
60
40
20
0
C
+ Vector
+ MARCH8
Chase time (hr)
VSV-G
Relative VSV-G
NS
*
**
***
150
100
50
0

Figure 4

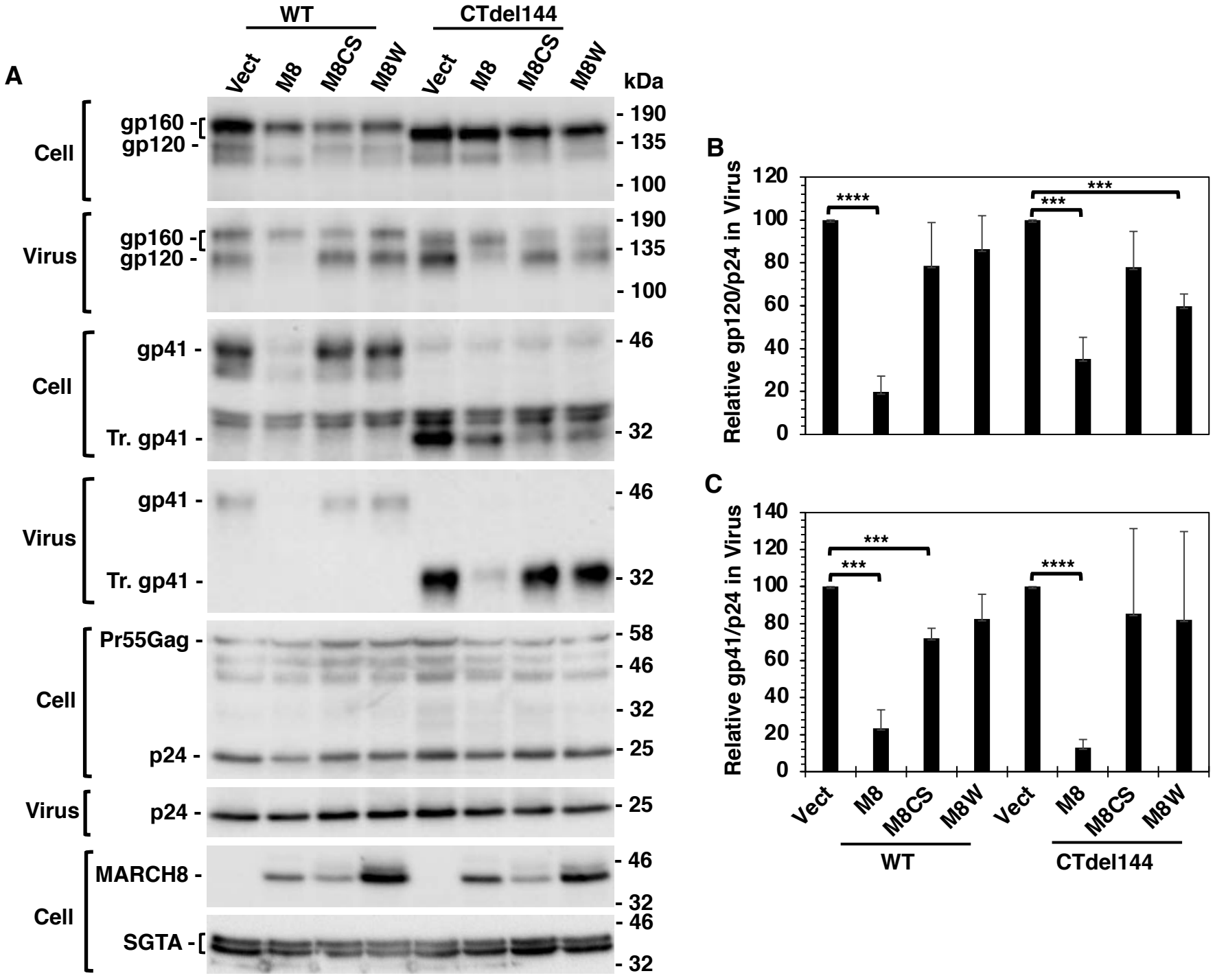
A
WT
CTdel144
Vect
M8
M8CS
M8W
kDa
Cell
gp160
gp120
190
135
100
Virus
gp41
Tr. gp41
46
32
Pr55Gag
58
25
p24
MARCH8
SGTA
B
Relative gp120/p24 in Virus
C
Relative gp41/p24 in Virus
****
***

Figure 5

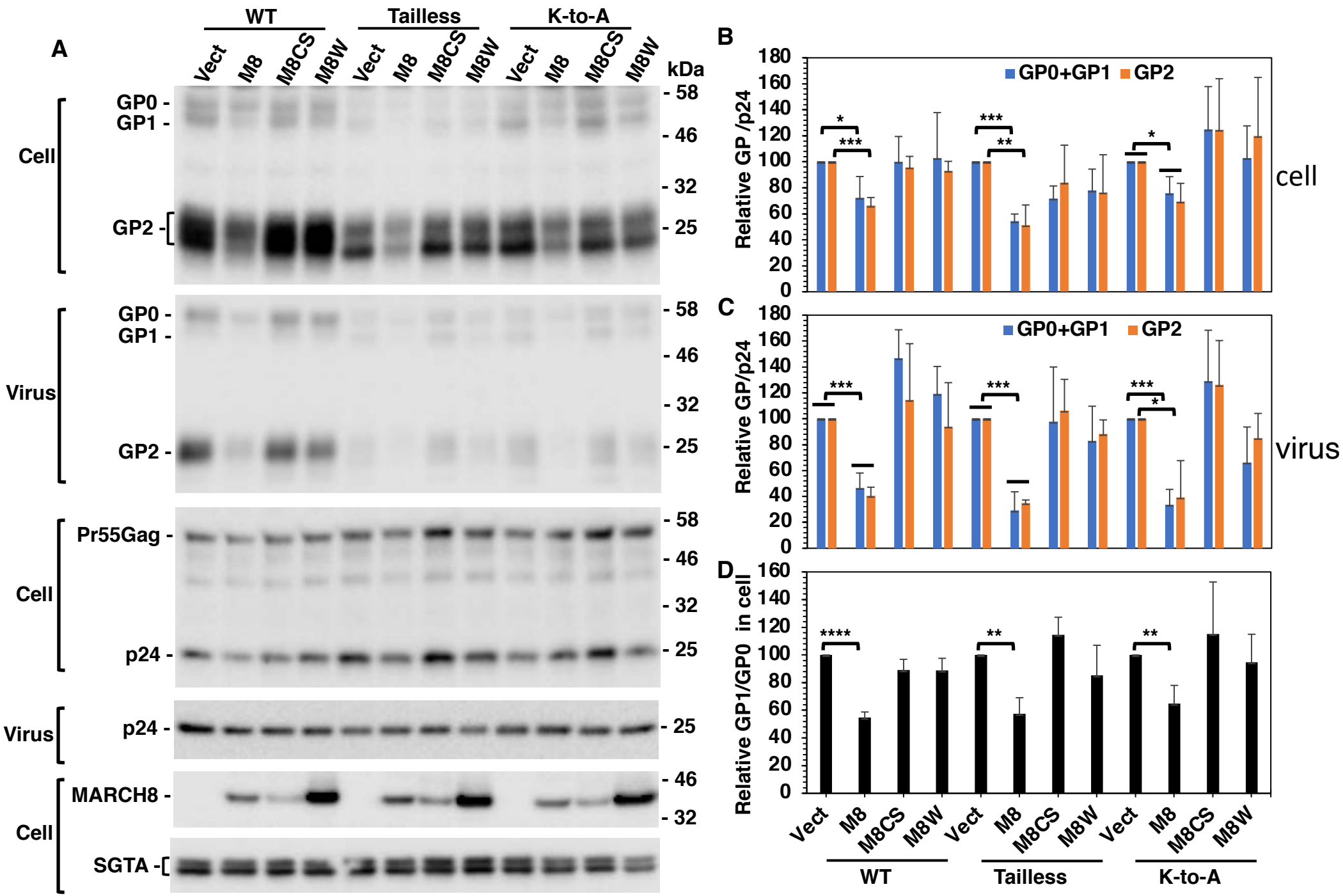
A
WT
Tailless
K-to-A
Vect
M8
M8CS
M8W
kDa
Cell
GP0
GP1
GP2
Virus
Pr55Gag
p24
MARCH8
SGTA
58
46
32
25
B
C
D
GP0+GP1
GP2
Relative GP /p24
Relative GP/p24
Relative GP1/GP0 in cell
cell
virus

Figure 6

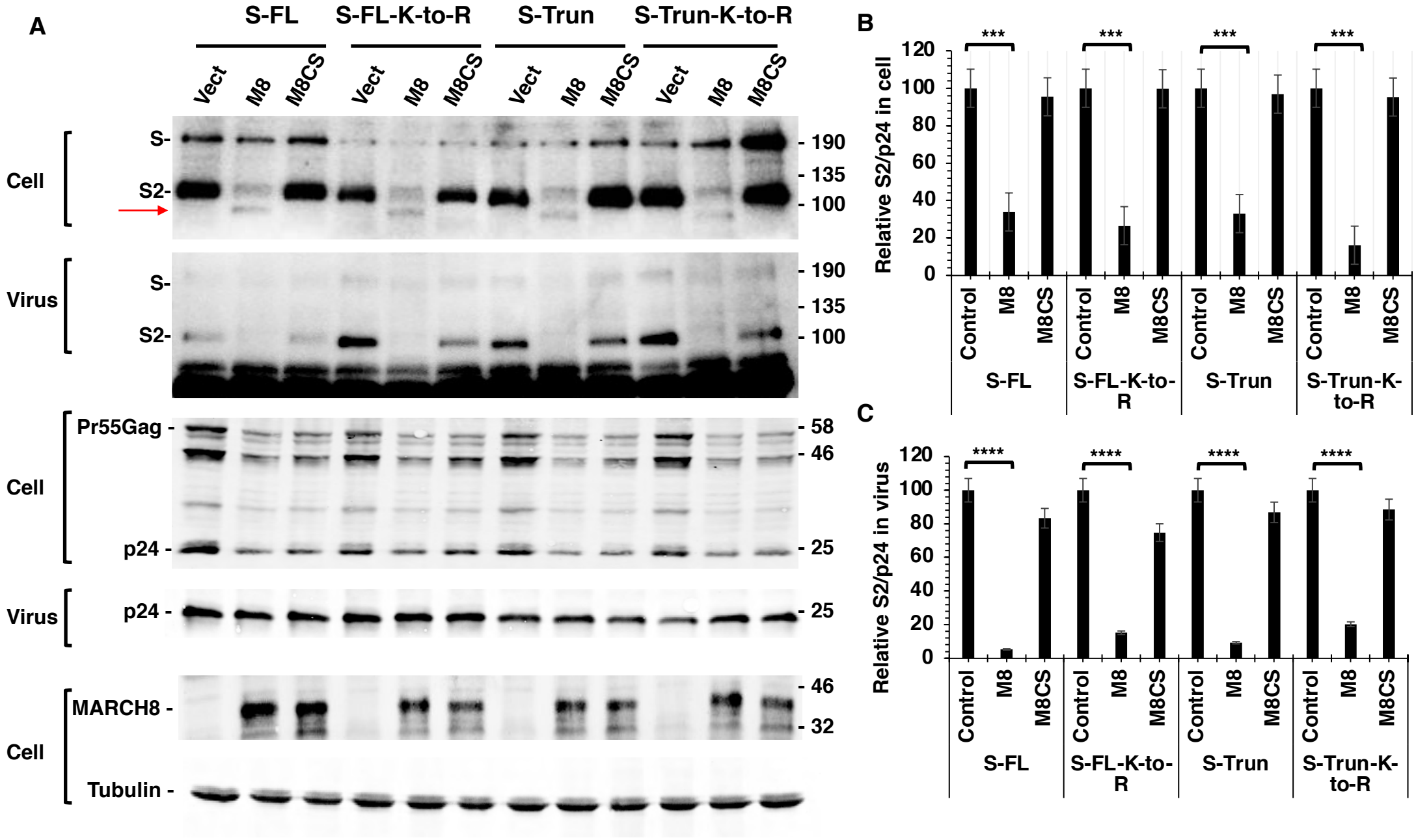
A
S-FL
S-FL-K-to-R
S-Trun
S-Trun-K-to-R
Vect
M8
M8CS
Cell
Virus
S-
S2-
190
135
100
Pr55Gag
p24
58
46
25
MARCH8
32
Tubulin
B
Relative S2/p24 in cell
***
Control
M8
M8CS
S-FL
S-FL-K-to-R
S-Trun
S-Trun-K-to-R
C
Relative S2/p24 in virus
****

Figure 7

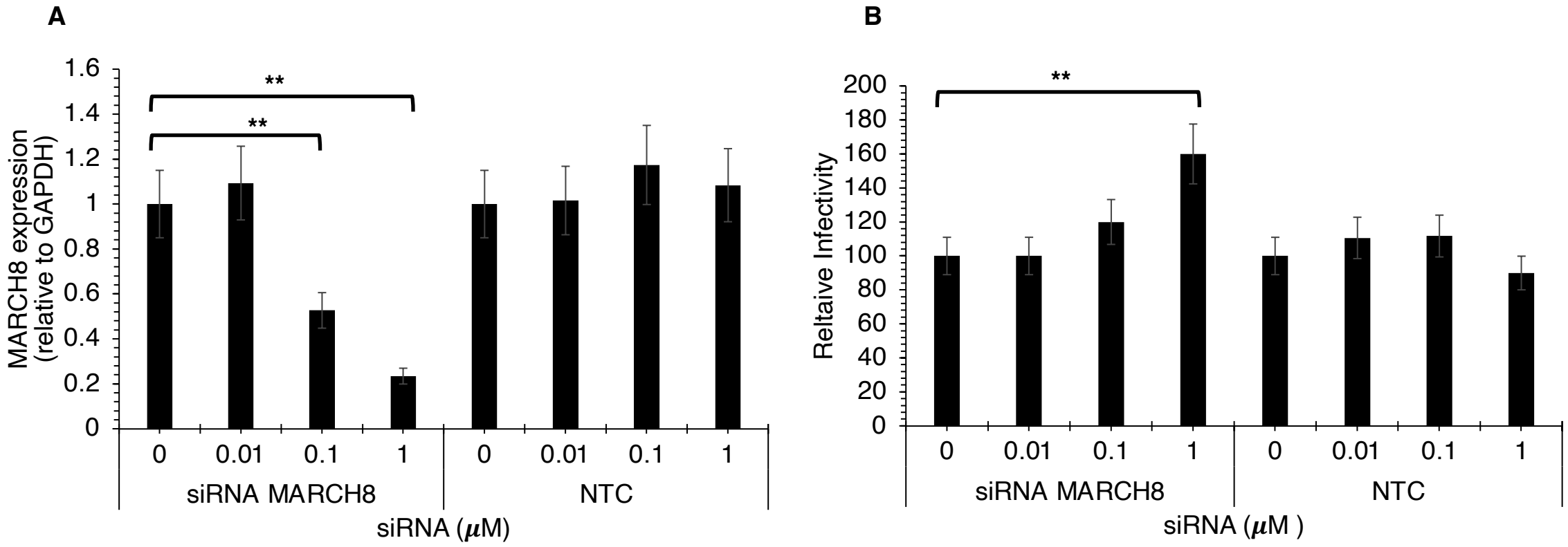
A
MARCH8 expression (relative to GAPDH)
1.6
1.4
1.2
1
0.8
0.6
0.4
0.2
0
**
**
0
0.01
0.1
1
0
0.01
0.1
1
siRNA MARCH8
NTC
siRNA (μM)
B
Reltaive Infectivity
200
180
160
140
120
100
80
60
40
20
0
**
0
0.01
0.1
1
0
0.01
0.1
1
siRNA MARCH8
NTC
siRNA (μM)

Figure 8

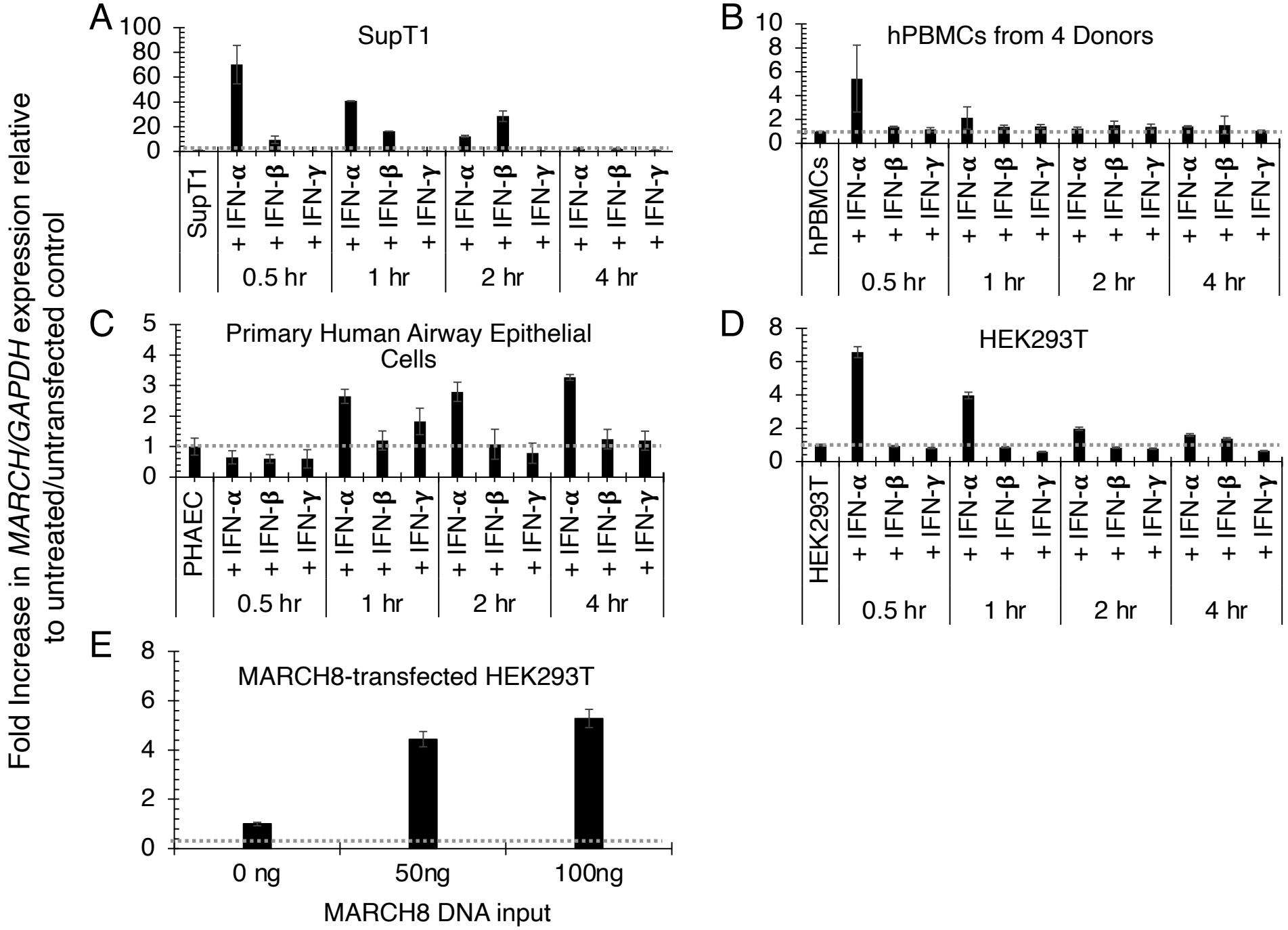
A
SupT1
B
hPBMCs from 4 Donors
C
Primary Human Airway Epithelial Cells
D
HEK293T
E
MARCH8-transfected HEK293T
Fold Increase in MARCH/GAPDH expression relative to untreated/untransfected control
SupT1
hPBMCs
PHAEC
HEK293T
+ IFN-α
+ IFN-β
+ IFN-γ
0.5 hr
1 hr
2 hr
4 hr
0 ng
50ng
100ng
MARCH8 DNA input

Figure 9A

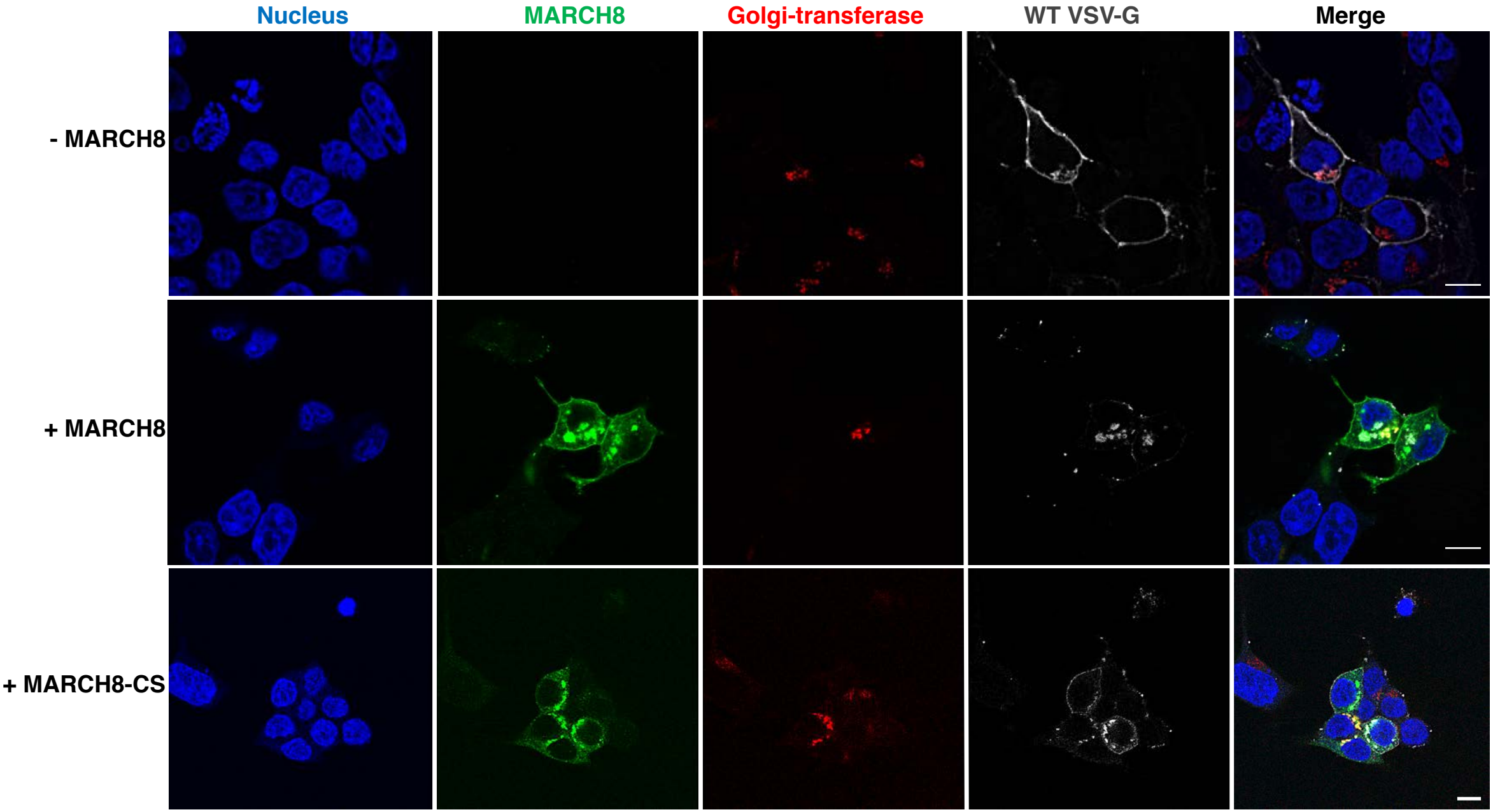
Nucleus
MARCH8
Golgi-transferase
WT VSV-G
Merge
- MARCH8
+ MARCH8
+ MARCH8-CS

Figure 9B

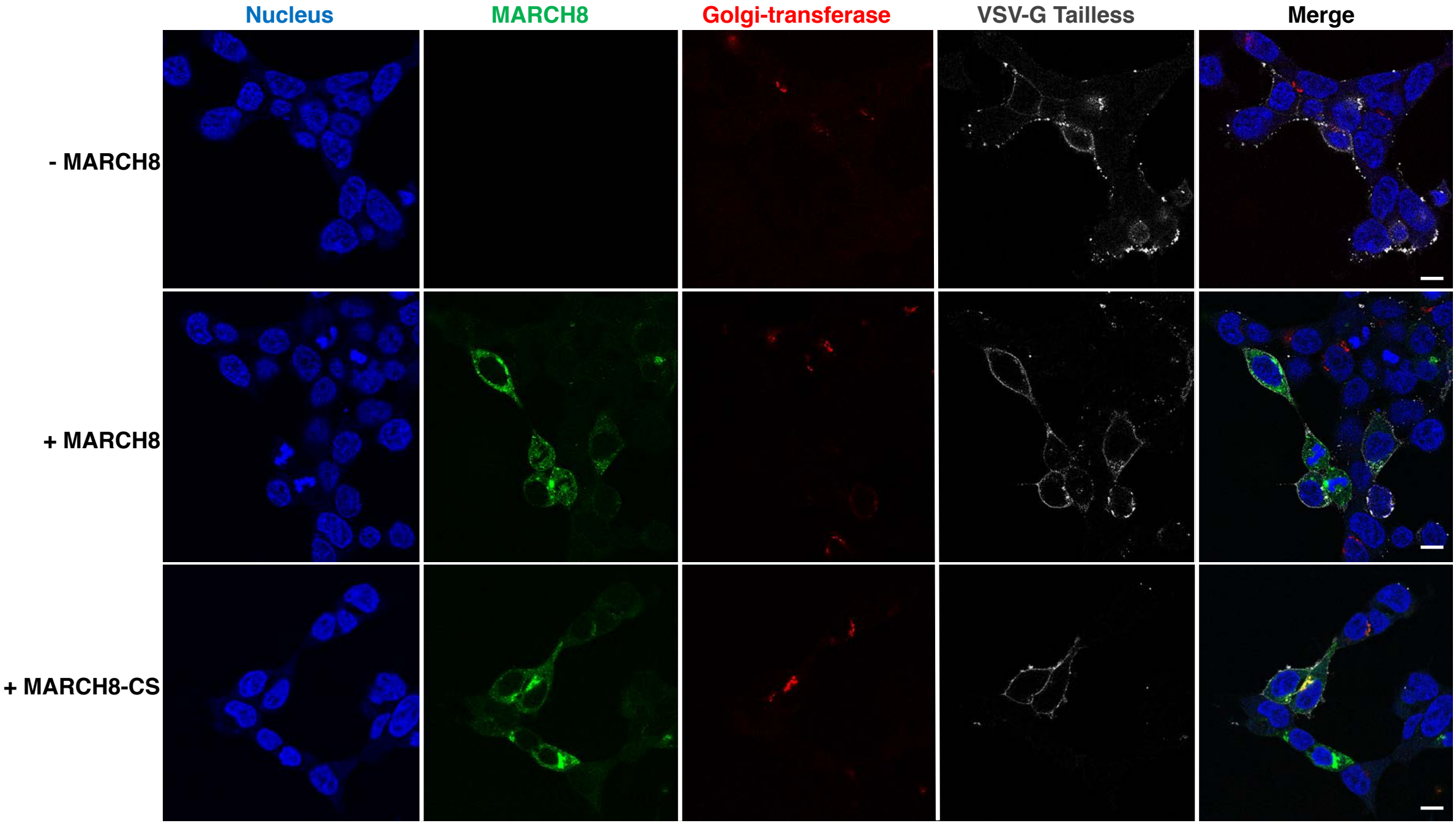
Nucleus
MARCH8
Golgi-transferase
VSV-G Tailless
Merge
- MARCH8
+ MARCH8
+ MARCH8-CS

Figure 9C

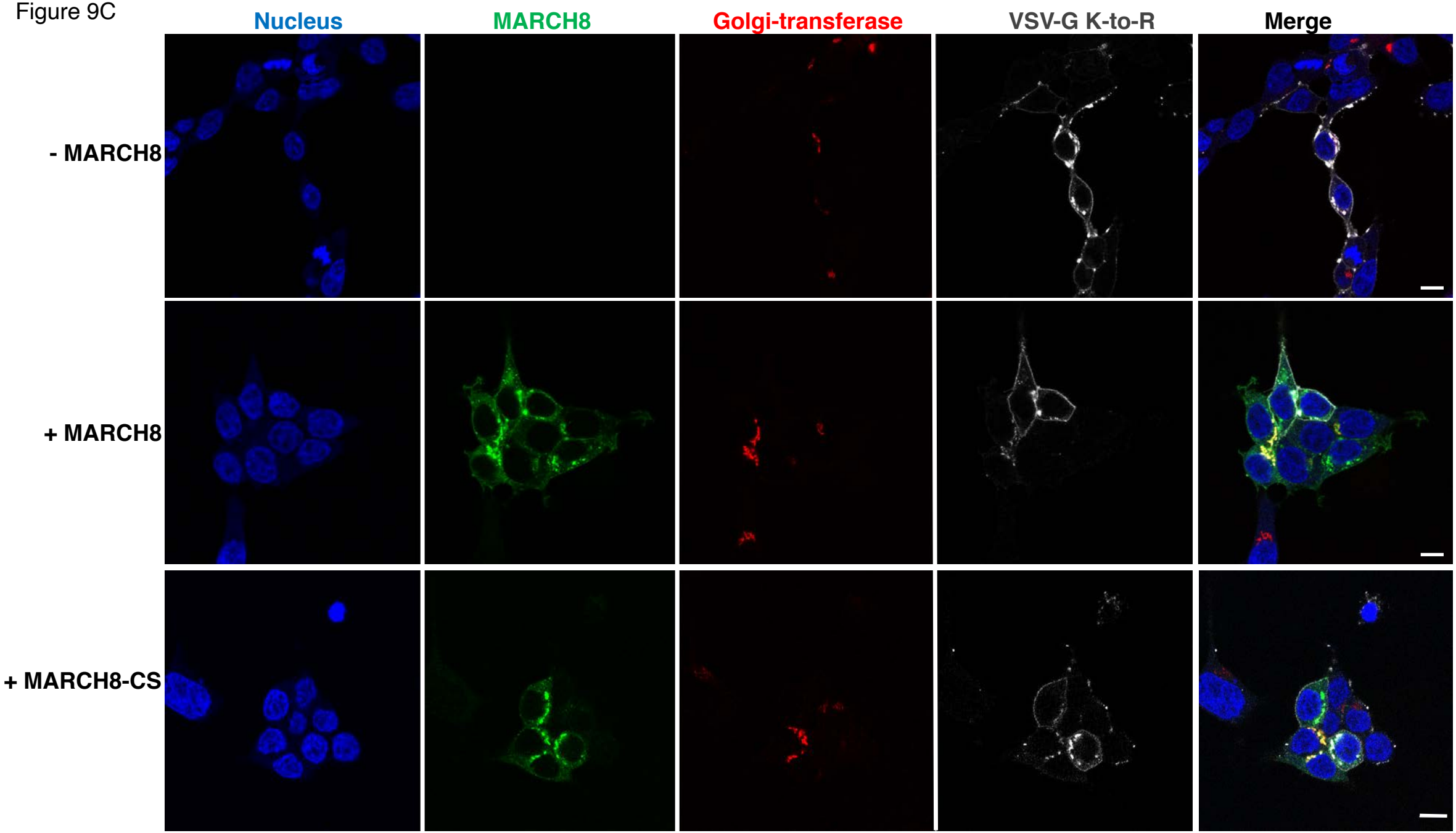
Nucleus
MARCH8
Golgi-transferase
VSV-G K-to-R
Merge
- MARCH8
+ MARCH8
+ MARCH8-CS

Figure 9D

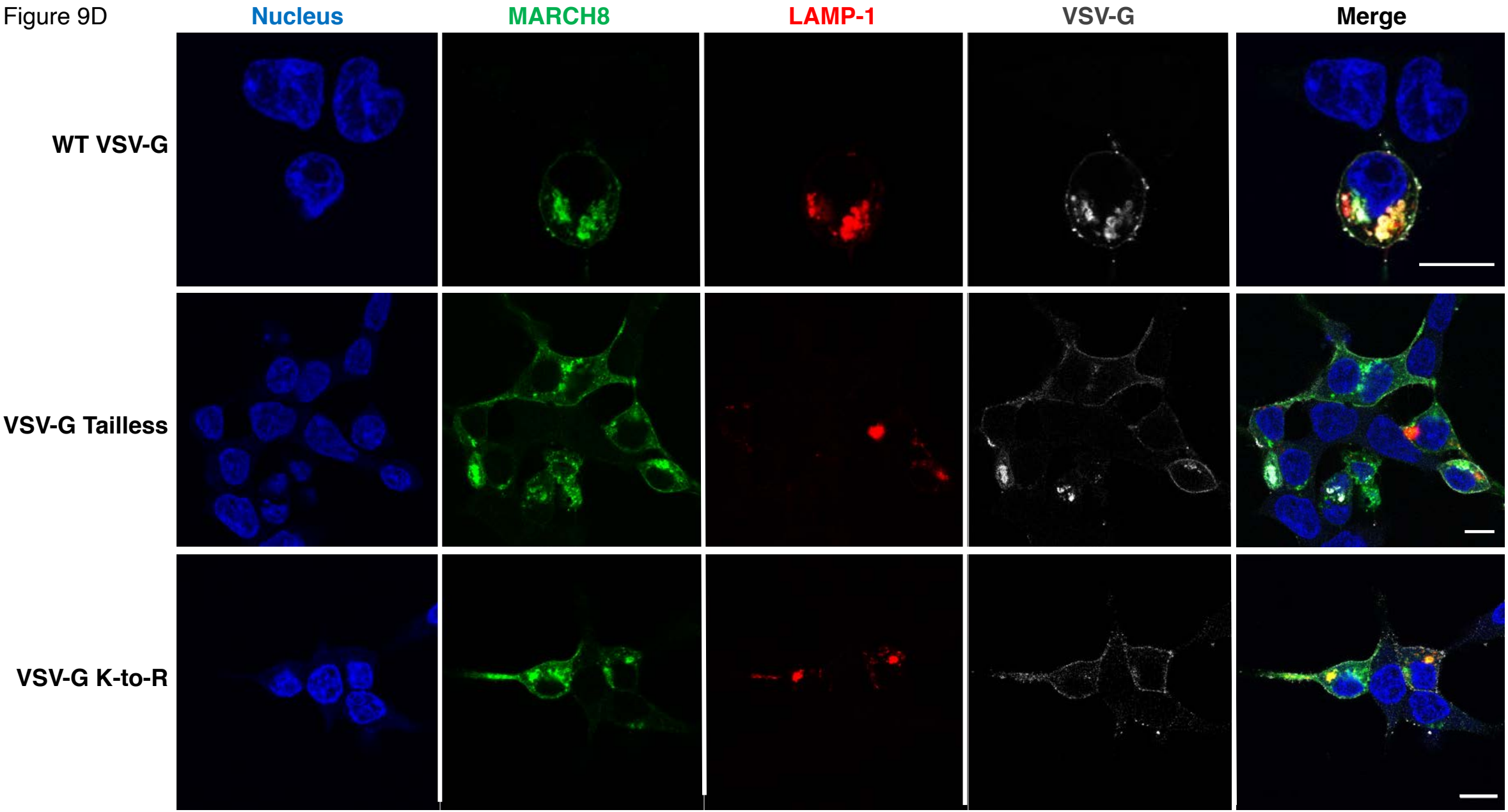
Nucleus
MARCH8
LAMP-1
VSV-G
Merge
WT VSV-G
VSV-G Tailless
VSV-G K-to-R

Figure 9E

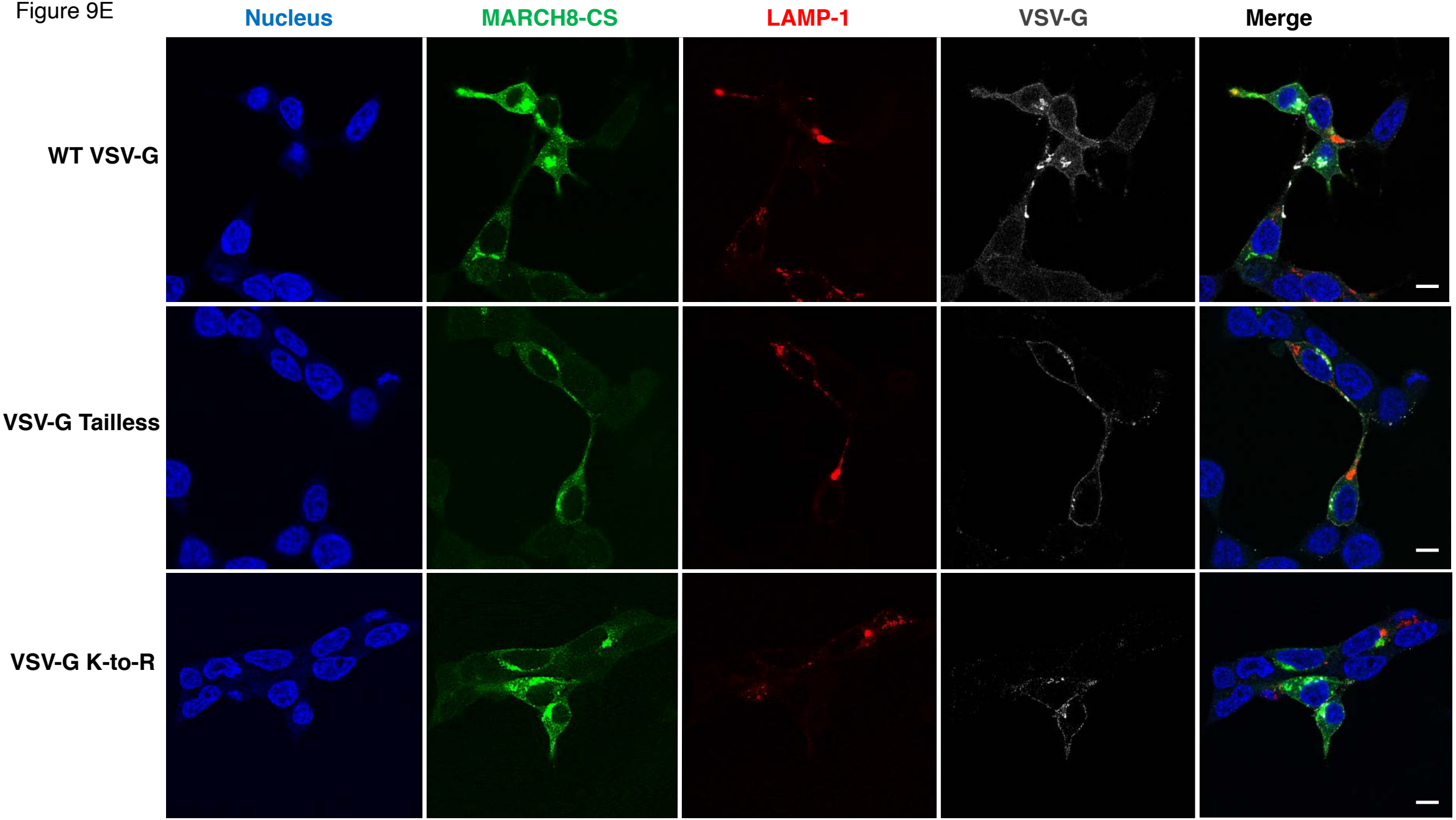
Nucleus
MARCH8-CS
LAMP-1
VSV-G
Merge
WT VSV-G
VSV-G Tailless
VSV-G K-to-R

Figure 10A

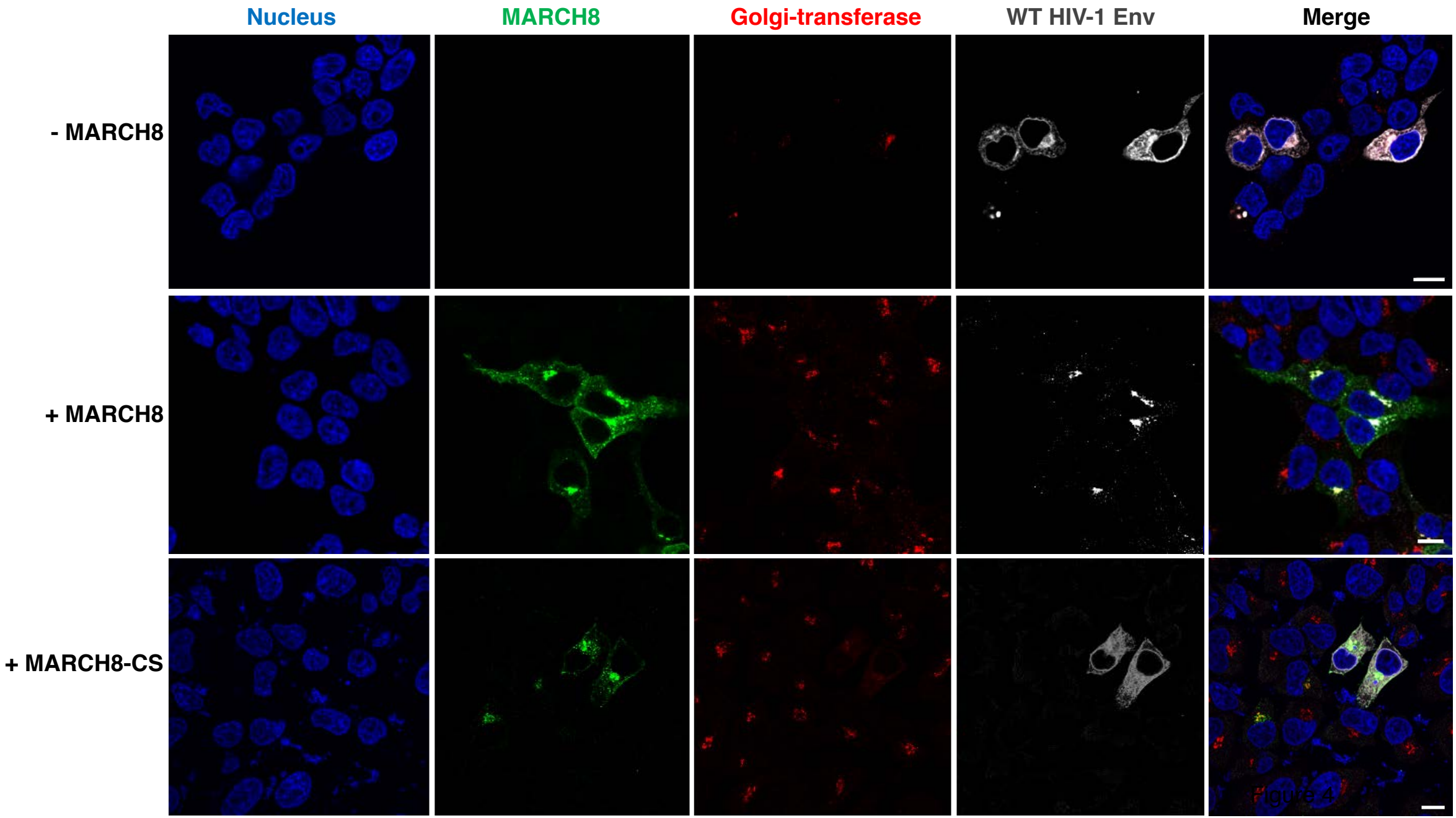
Nucleus
MARCH8
Golgi-transferase
WT HIV-1 Env
Merge
- MARCH8
+ MARCH8
+ MARCH8-CS
Figure 4

Figure 10B

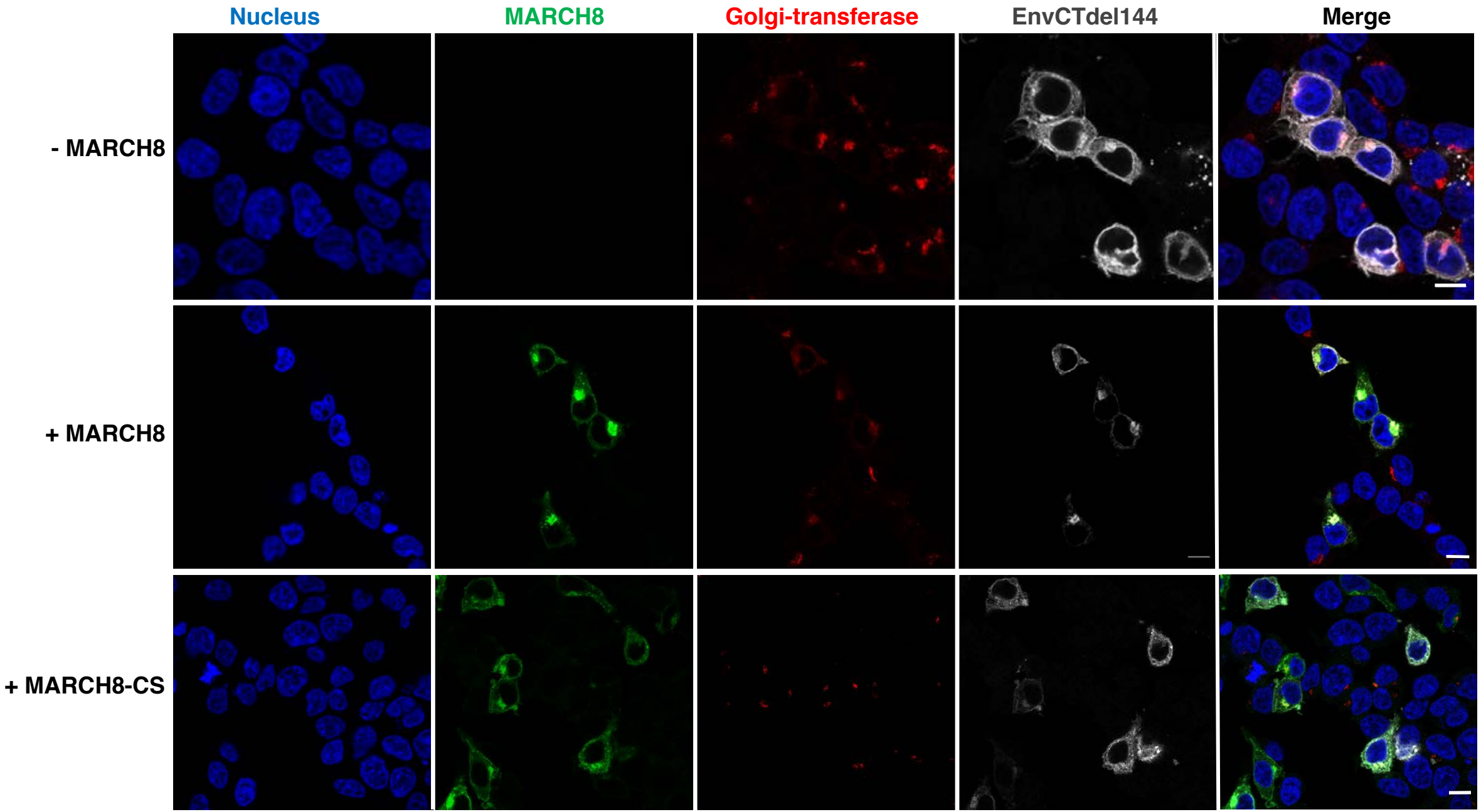
Nucleus
MARCH8
Golgi-transferase
EnvCTdel144
Merge
- MARCH8
+ MARCH8
+ MARCH8-CS

Figure 10C

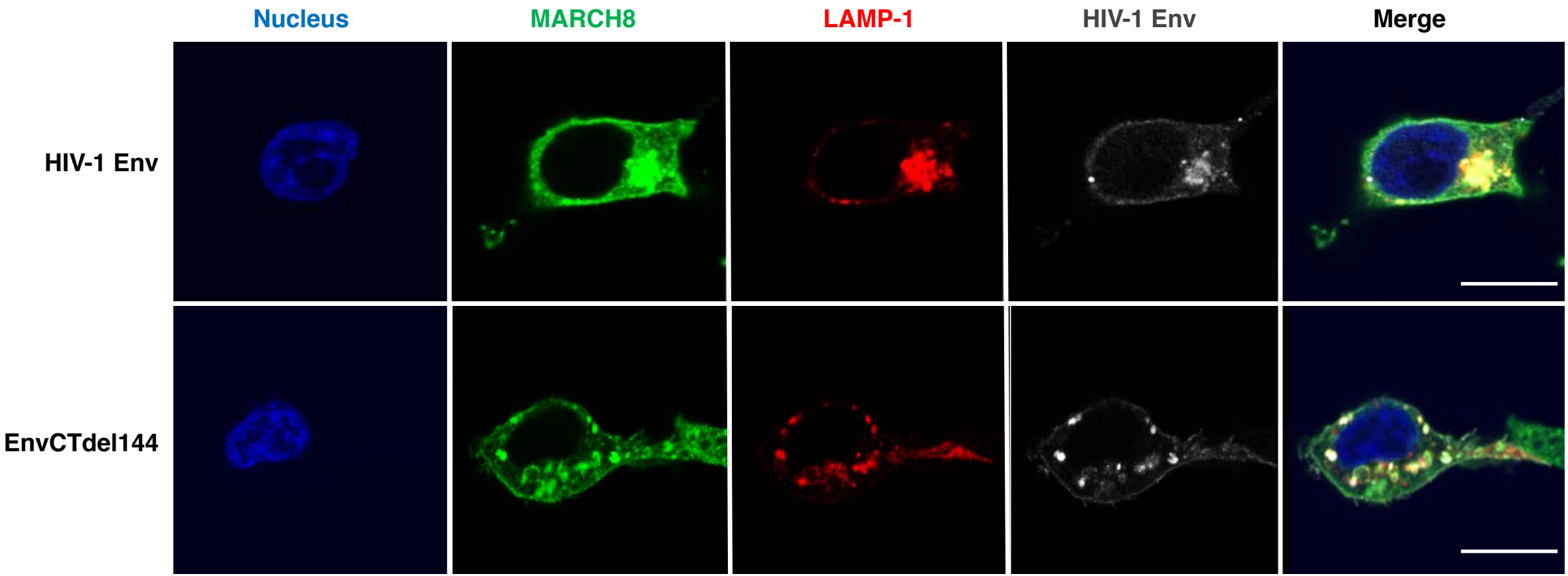

Figure 10D

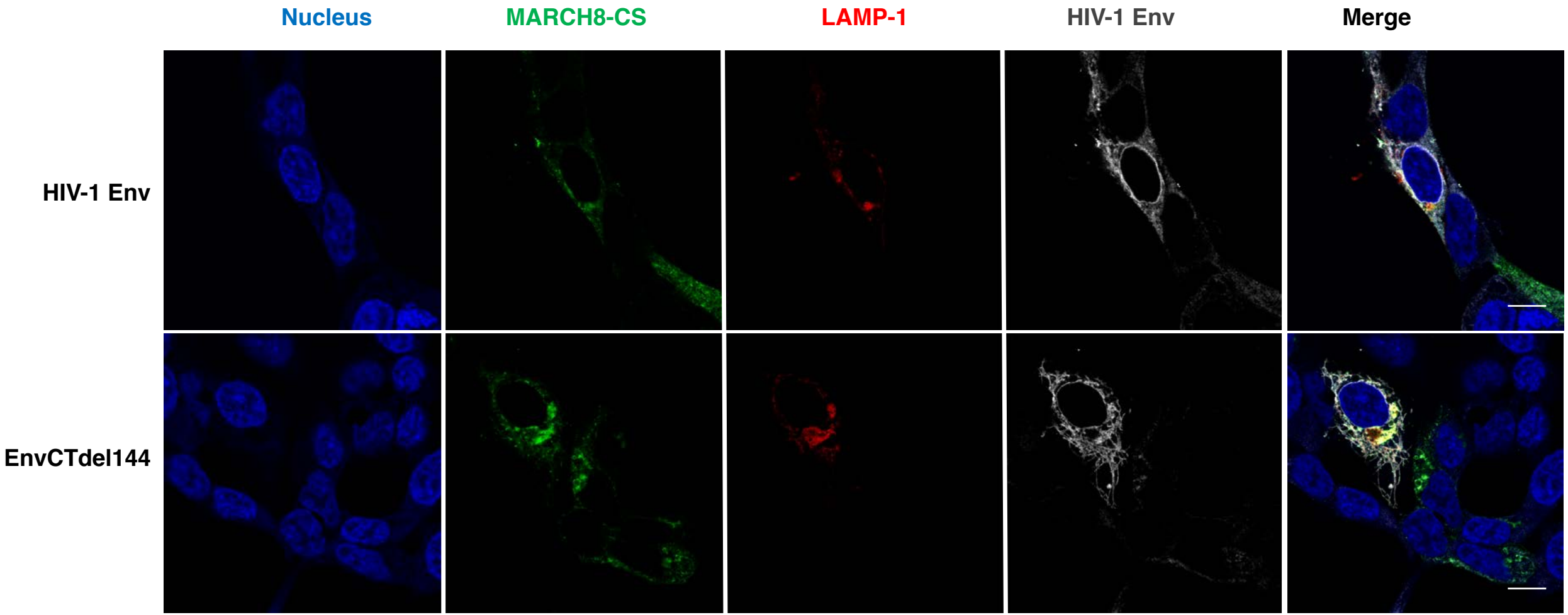
Nucleus
MARCH8-CS
LAMP-1
HIV-1 Env
Merge
HIV-1 Env
EnvCTdel144

Figure 11A

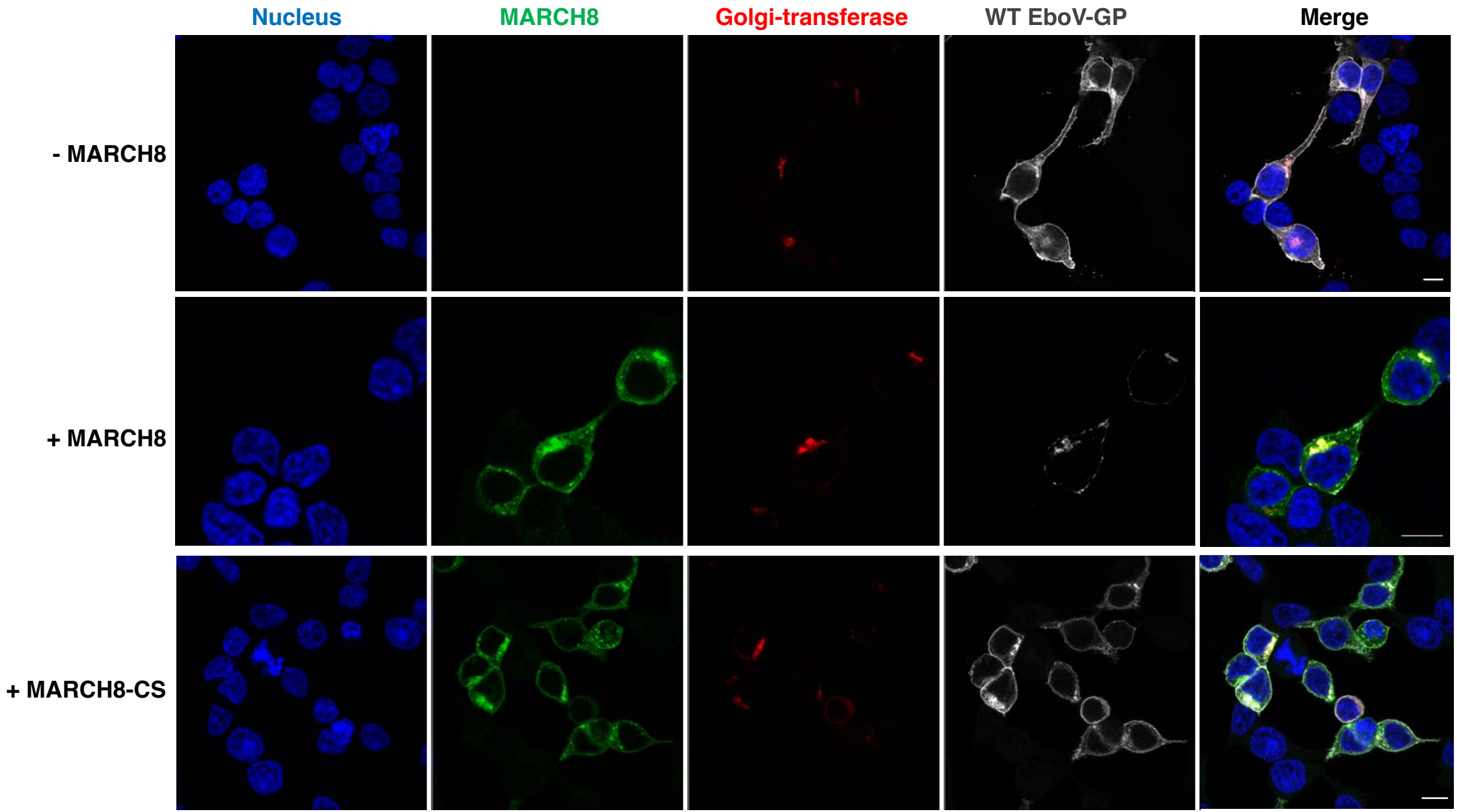
Nucleus
MARCH8
Golgi-transferase
WT EboV-GP
Merge
- MARCH8
+ MARCH8
+ MARCH8-CS

Figure 11B

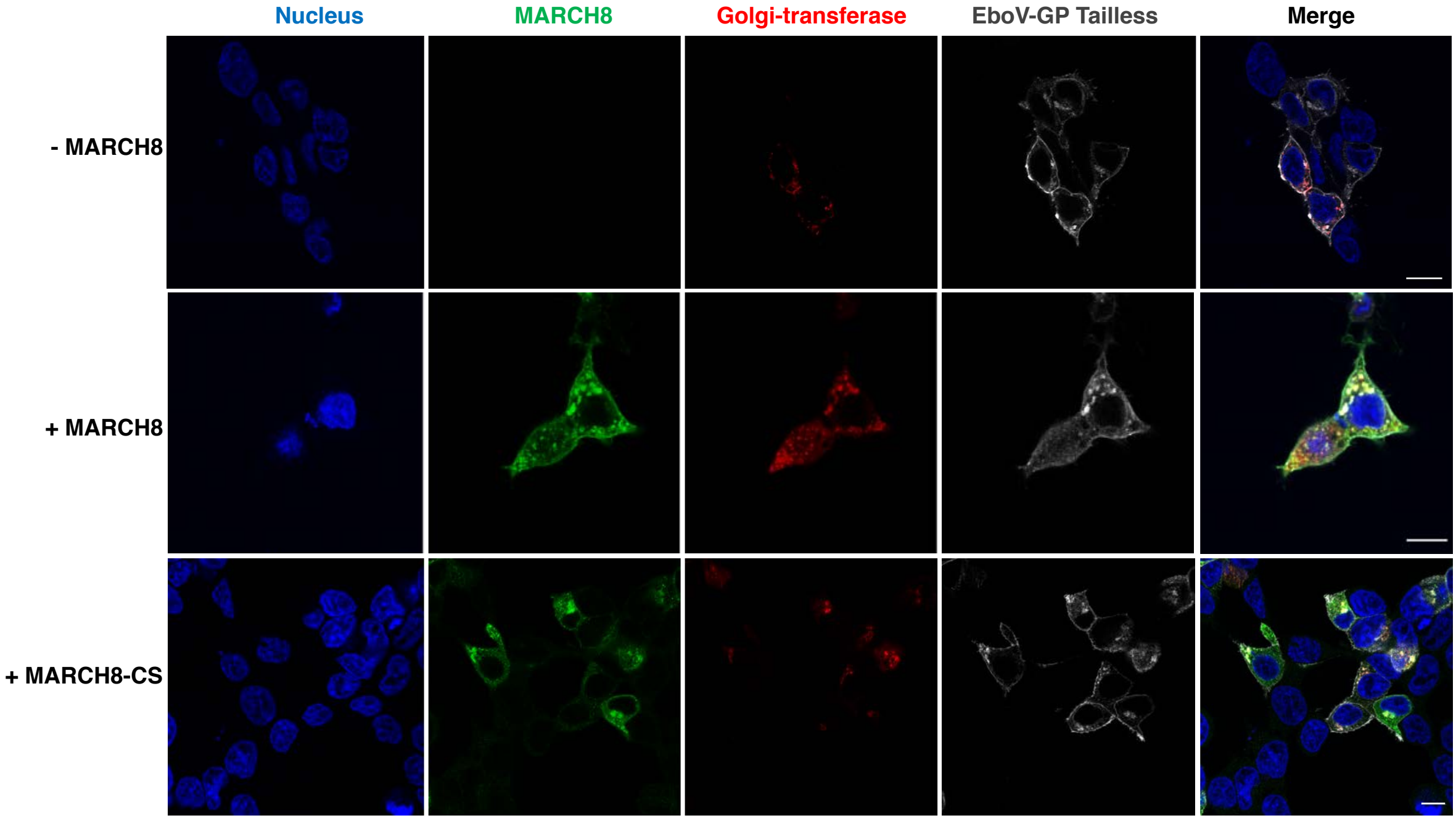
Nucleus
MARCH8
Golgi-transferase
EboV-GP Tailless
Merge
- MARCH8
+ MARCH8
+ MARCH8-CS

Figure 11C

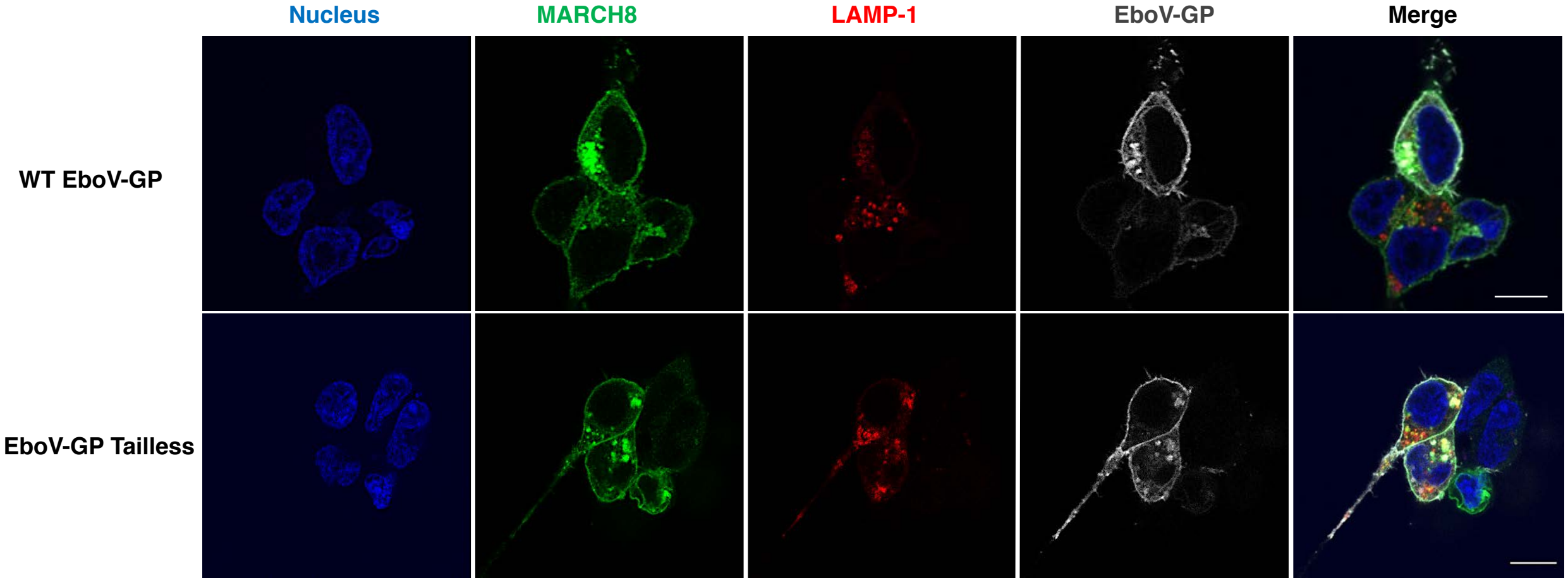
Nucleus
MARCH8
LAMP-1
EboV-GP
Merge
WT EboV-GP
EboV-GP Tailless

Figure 11D

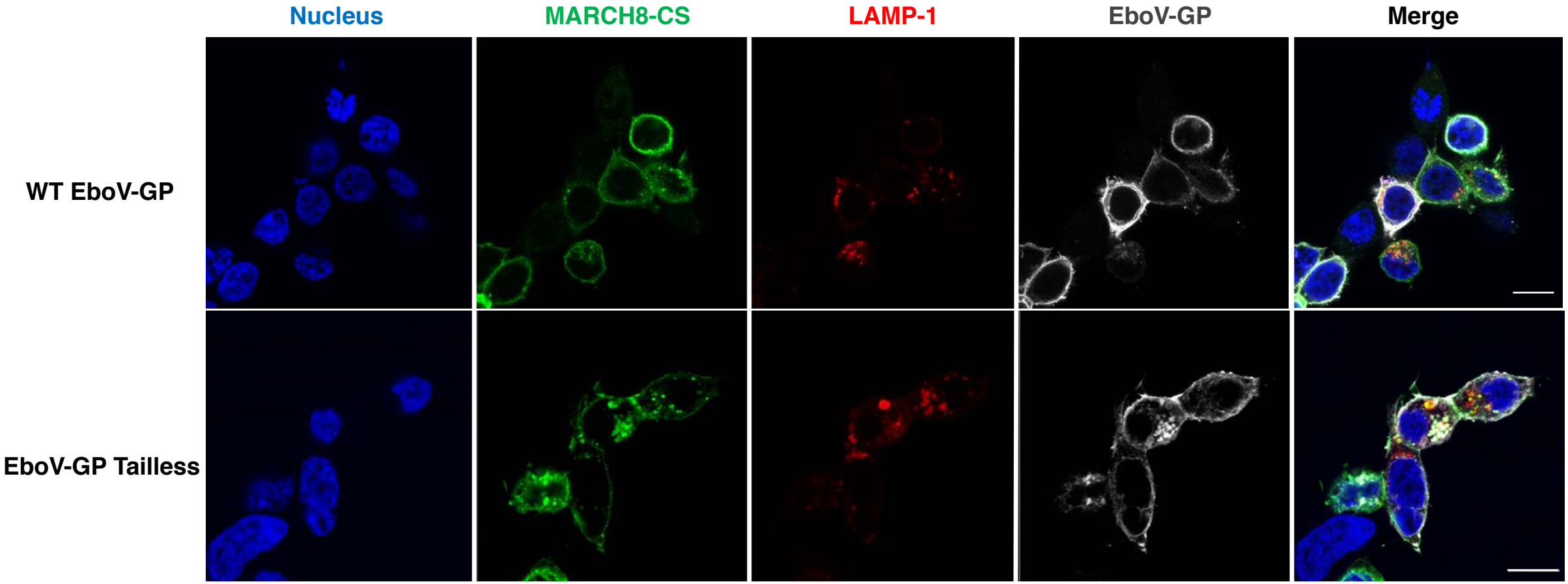
Nucleus
MARCH8-CS
LAMP-1
EboV-GP
Merge
WT EboV-GP
EboV-GP Tailless

Figure 12A

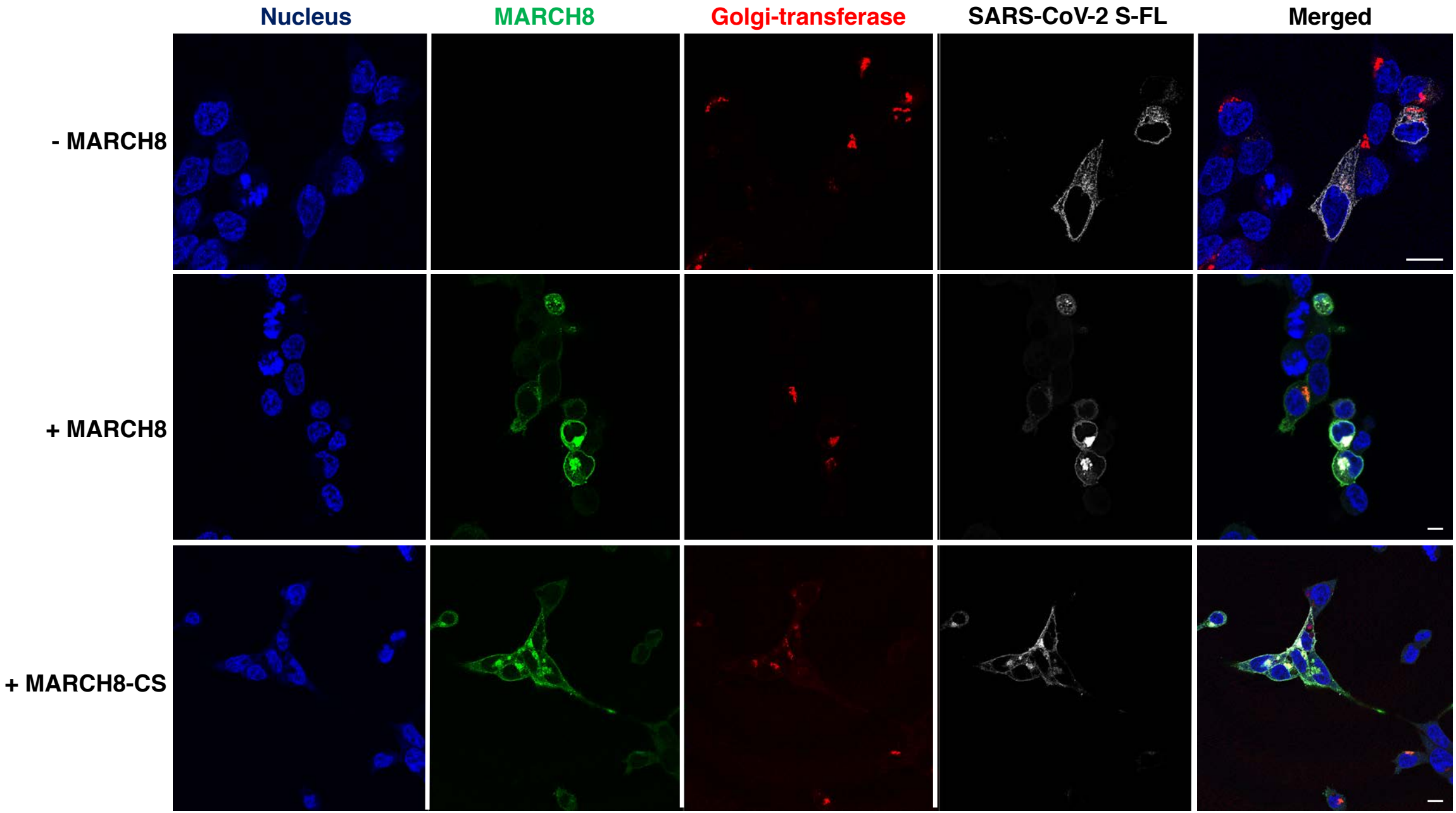
Nucleus
MARCH8
Golgi-transferase
SARS-CoV-2 S-FL
Merged
- MARCH8
+ MARCH8
+ MARCH8-CS

Figure 12B

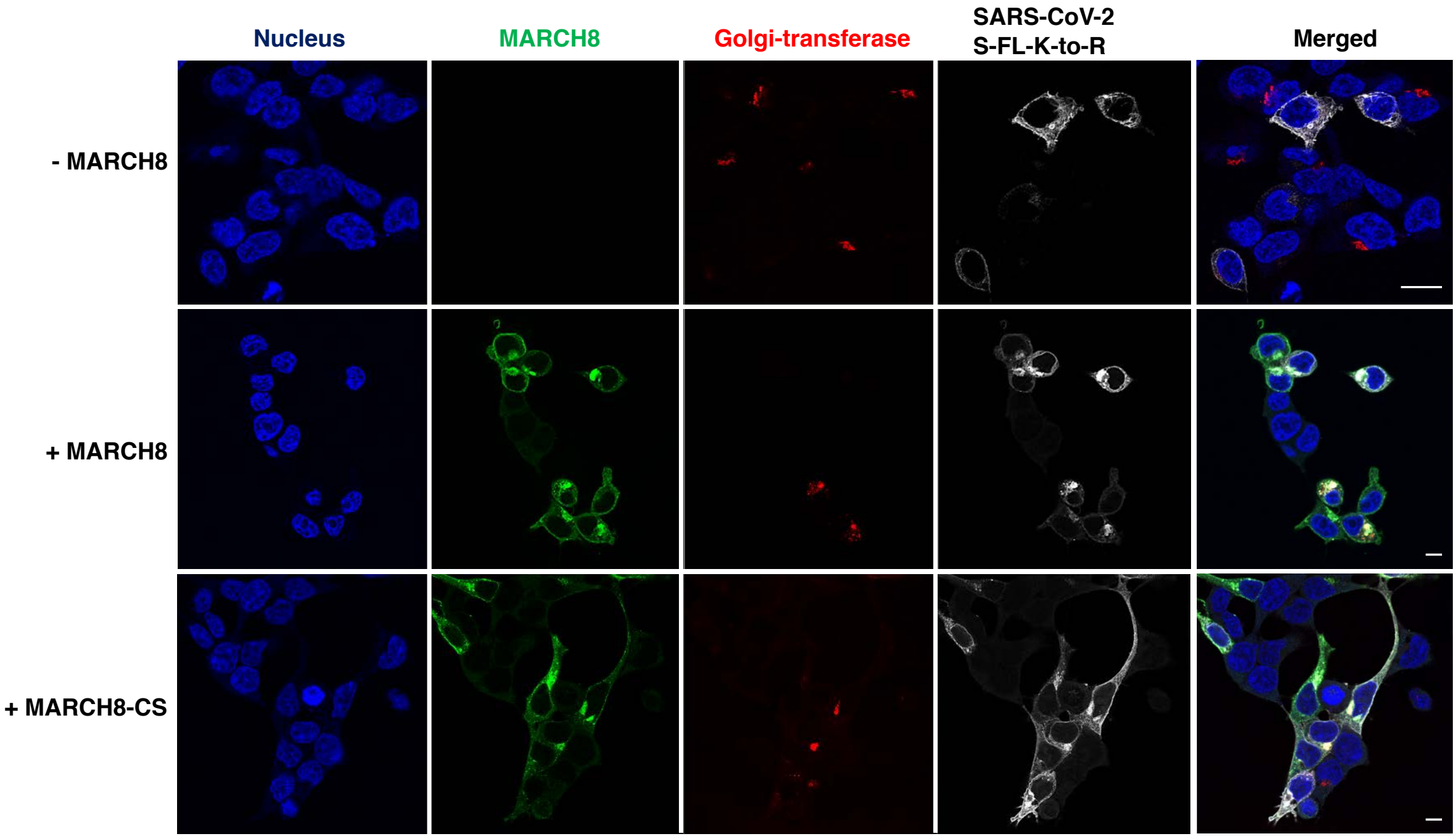
Nucleus
MARCH8
Golgi-transferase
SARS-CoV-2
S-FL-K-to-R
Merged
- MARCH8
+ MARCH8
+ MARCH8-CS

Figure 12C

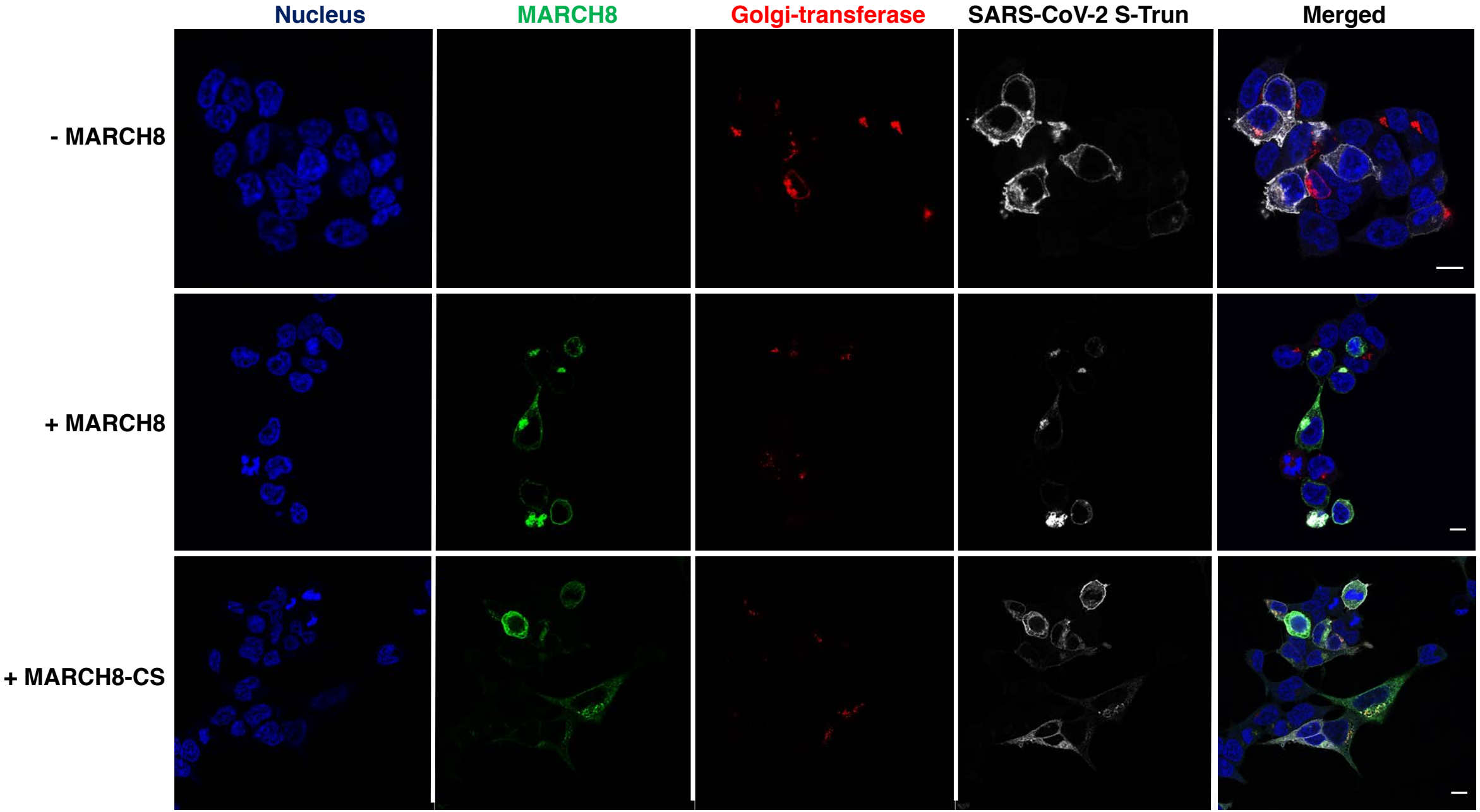
Nucleus
MARCH8
Golgi-transferase
SARS-CoV-2 S-Trun
Merged
- MARCH8
+ MARCH8
+ MARCH8-CS

Figure 12D

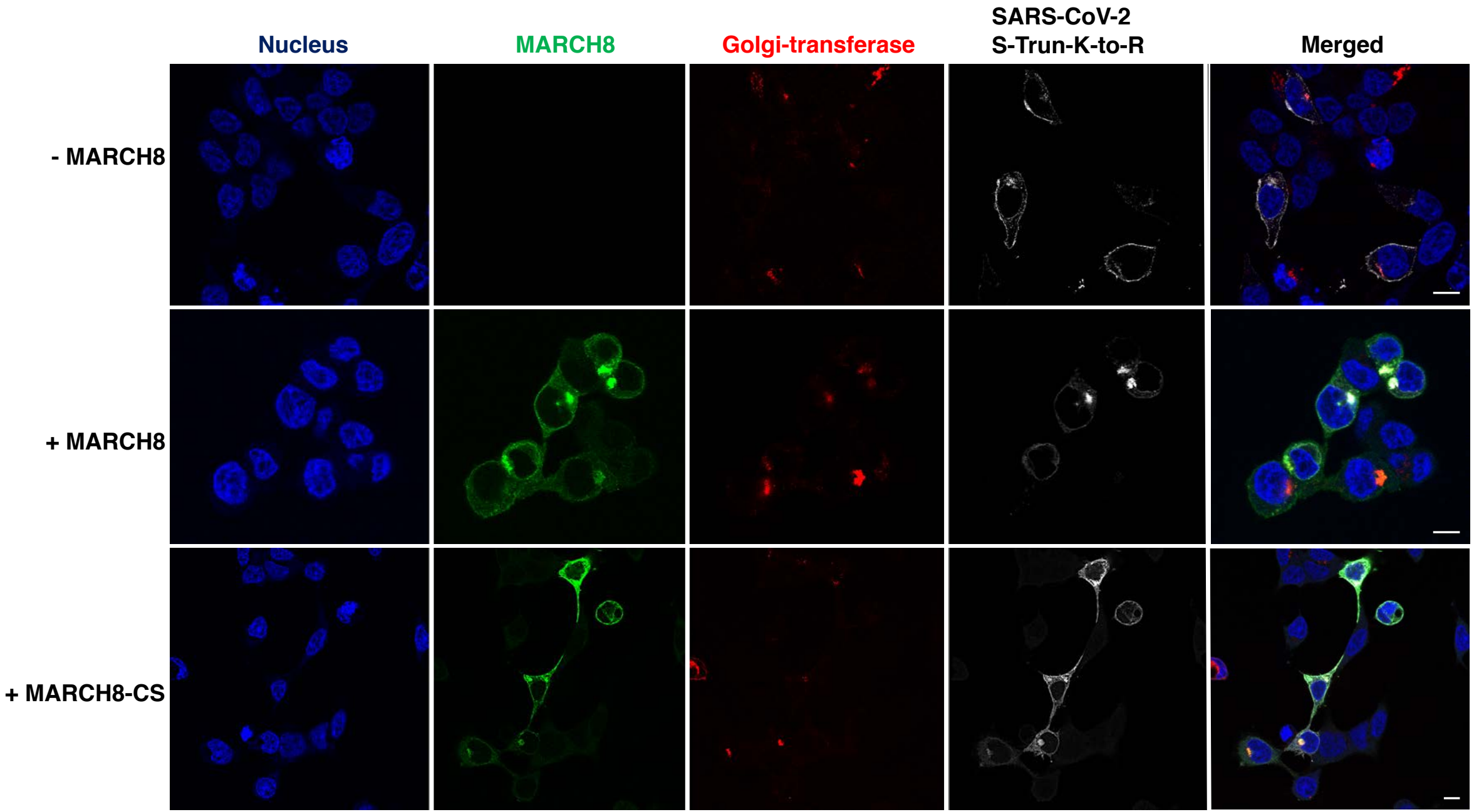
Nucleus
MARCH8
Golgi-transferase
SARS-CoV-2
S-Trun-K-to-R
Merged
- MARCH8
+ MARCH8
+ MARCH8-CS

Figure 12E

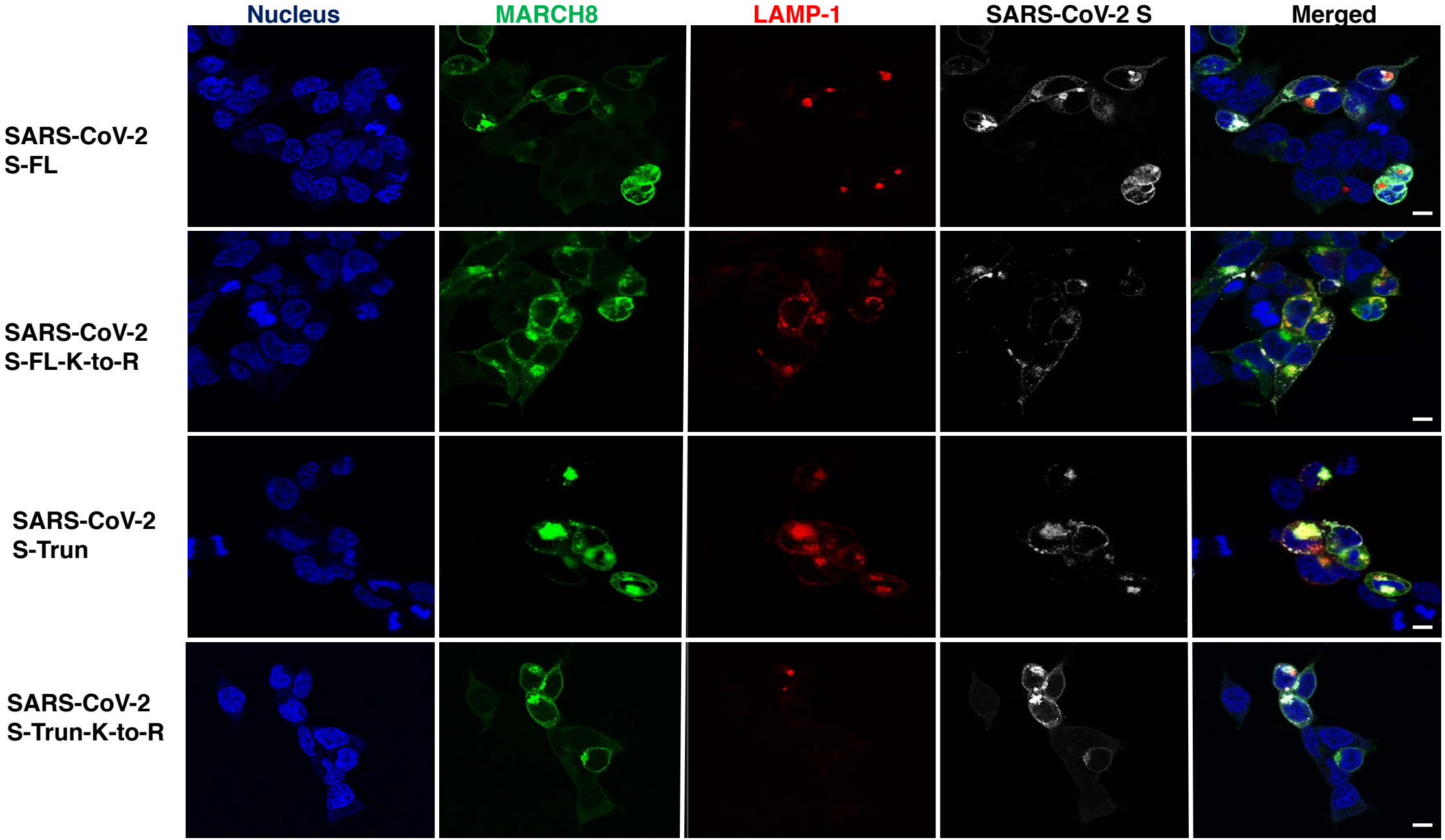
Nucleus
MARCH8
LAMP-1
SARS-CoV-2 S
Merged
SARS-CoV-2 S-FL
SARS-CoV-2 S-FL-K-to-R
SARS-CoV-2 S-Trun
SARS-CoV-2 S-Trun-K-to-R

Figure 12F

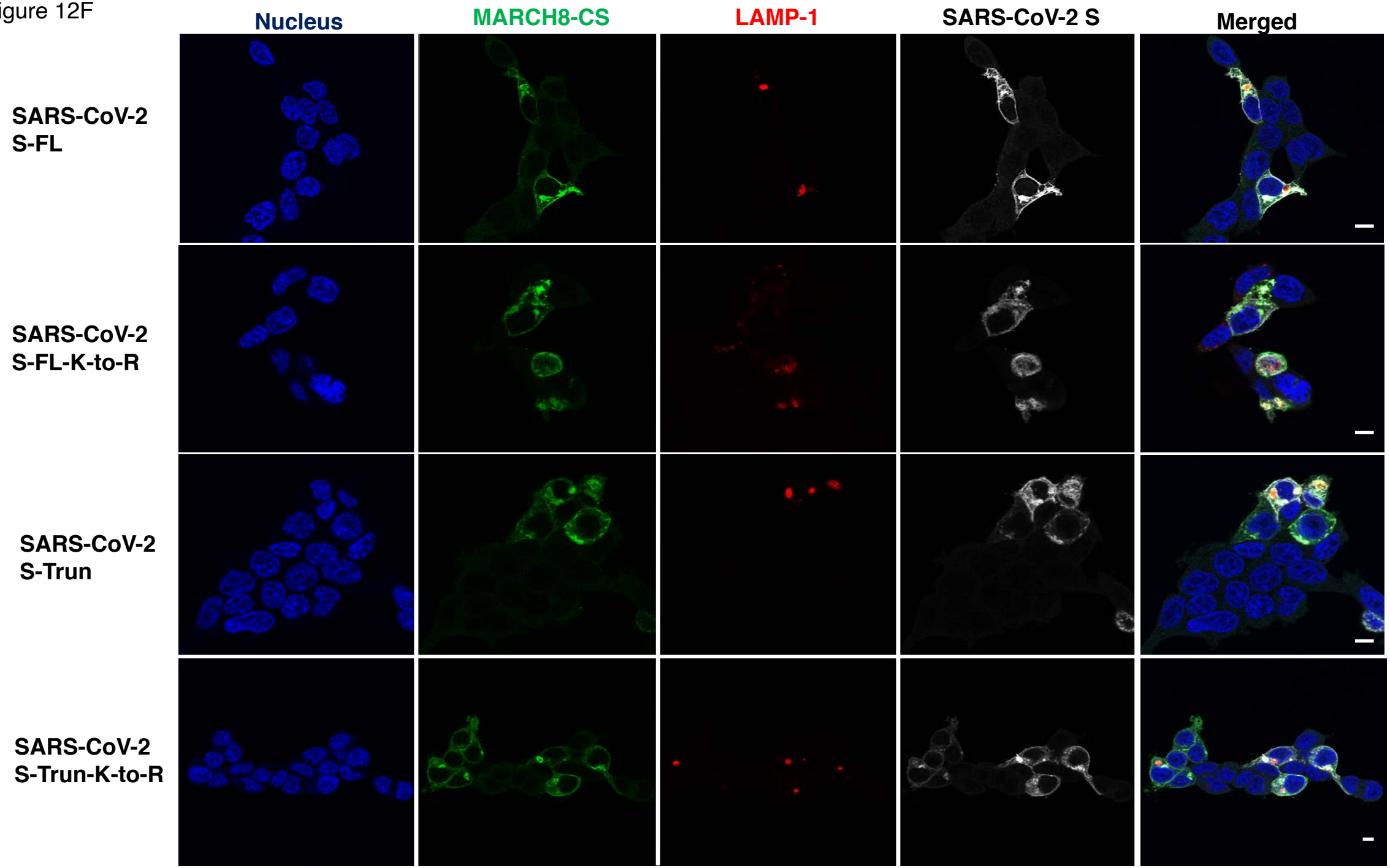
Nucleus
MARCH8-CS
LAMP-1
SARS-CoV-2 S
Merged
SARS-CoV-2 S-FL
SARS-CoV-2 S-FL-K-to-R
SARS-CoV-2 S-Trun
SARS-CoV-2 S-Trun-K-to-R